



THE UNIVERSITY *of* EDINBURGH

Edinburgh Research Explorer

Does pebble abrasion influence detrital age population statistics? A numerical investigation of natural datasets

Citation for published version:

Lavarini ferreira, C, Attal, M, da Costa Filho, CA & Kirstein, L 2018, 'Does pebble abrasion influence detrital age population statistics? A numerical investigation of natural datasets', *Journal of Geophysical Research: Earth Surface*. <https://doi.org/10.1029/2018JF004610>

Digital Object Identifier (DOI):

[10.1029/2018JF004610](https://doi.org/10.1029/2018JF004610)

Link:

[Link to publication record in Edinburgh Research Explorer](#)

Document Version:

Peer reviewed version

Published In:

Journal of Geophysical Research: Earth Surface

Publisher Rights Statement:

©2018. American Geophysical Union. All Rights Reserved.

General rights

Copyright for the publications made accessible via the Edinburgh Research Explorer is retained by the author(s) and / or other copyright owners and it is a condition of accessing these publications that users recognise and abide by the legal requirements associated with these rights.

Take down policy

The University of Edinburgh has made every reasonable effort to ensure that Edinburgh Research Explorer content complies with UK legislation. If you believe that the public display of this file breaches copyright please contact openaccess@ed.ac.uk providing details, and we will remove access to the work immediately and investigate your claim.



Does pebble abrasion influence detrital age population statistics? A numerical investigation of natural datasets

C. Lavarini^{1*}, M. Attal¹, C. A. da Costa Filho¹, and L.A. Kirstein¹

¹School of GeoSciences, University of Edinburgh, James Hutton Road, Edinburgh, EH9 3FE, Scotland, UK.

Key Points:

- Pebble abrasion can distort the mineralogy of fluvial sands and ultimately the statistics of detrital age populations derived from them.
- Simulations show that abrasion is able to produce detrital age distortion but less than spatially variable erosion and mineral fertility.
- Simulations with empirical data show that relative erosion rates derived from age populations are different when accounting for abrasion.

* Corresponding author: Chrystiann Lavarini, c.lavarini@ed.ac.uk

Abstract

Pebble abrasion is a key factor controlling the release of minerals into sand, but few attempts have been made to model how it could influence the liberation of minerals into the size fraction used in detrital geochronology. We perform a series of experiments with an abrasion model to test this influence using natural and synthetic datasets. Our results demonstrate that pebble abrasion can change the zircon mixing proportions of upstream source units as well as the age distribution of mixed fluvial sands. This change is particularly significant when there is strong contrast in rock resistance within the watershed. Pebble abrasion is one of many factors that can change the mixing proportion of sands, including hillslope gravel supply, erosion rates, and mineral fertility. In our study case (Marsyandi watershed, Himalaya), the abrasion model predicts age distributions that are statistically indistinguishable from those predicted by a no-abrasion model. However, the relative erosion rates estimated by our model largely differ from the results of a no-abrasion model, and are closer to those from other studies that suggest a strong correlation between modern erosion rates, tectonics and precipitation intensity in the Marsyandi watershed. These findings highlight that, even in cases where there is no statistical evidence of change between the modelled age distributions, abrasion can affect the erosion rates estimated from them. Therefore, quantifying the influence of abrasion on sand production is an essential step not only to predict mixing proportions but also to accurately retrieve erosion rates from the measured grain age distributions.

Keywords: sediment, detrital methods, abrasion, provenance, bias, erosion, geochronology, zircon.

1 Introduction

Minerals rich in uranium and thorium contain vital clues to unravelling Earth's history. More resistant minerals such as zircon behave as Earth's timekeepers as they can retain information even after crustal or sediment recycling, and so are key tools to reconstruct ancient geological events (e.g., Amelin et al., 1999; Mojzsis et al., 2001; Wilde et al., 2001). For this reason, detrital zircon has been extensively used in investigations about the growth and evolution of continents (e.g., Iizuka et al., 2010; Dhuime et al., 2012; Oliver et al., 2014), documenting sub-glacial erosion (e.g., Cox et al., 2010; Tochilin et al., 2012; Thomson et al., 2013) as well as reconstructing sediment provenance and drainage development (e.g., Singh et al., 2008; Kirstein et al., 2009, 2013; Alizai et al., 2011; Gehrels et al., 2011; Blum and Pecha, 2014).

But how representative are the sampled grains of the original system? We should not ignore this perennial question if we are to have confidence in our interpretation of preserved sedimentary deposits and what they represent. The importance of investigating source-to-sink processes that may have influenced the preservation of grains is increasingly being recognized (Garzanti et al., 2009; Lukens et al., 2016). Potential biases, if measurable, could have profound effects on the way in which we interpret the sedimentary record. As a result, a number of studies have focused on how different processes such as sediment generation on hillslopes (e.g., Riebe et al., 2015; Lukens et al., 2016), transport in river channels (e.g., Garzanti et al., 2008, 2009; Lawrence et al., 2011a) and sediment mixing in watersheds (Haddadchi et al., 2013, 2014) can affect the way we use detrital information.

At the same time, numerical models have increasingly been applied as a tool to unravel the source of zircons in modern rivers (Sundell and Saylor, 2017). Several of these models apply a forward mixing approach, whereby empirical observations such as exposure area and zircon fertility (i.e. the concentration of the mineral of interest in the source area) are used to generate an artificial grain age probability density function which is compared to the best fit of the measured grain age distribution (e.g., Saylor et al., 2013; Kimbrough et al., 2015; Licht et al., 2016; Sharman and Johnstone, 2017). There is often a mismatch between the model-predicted and best-fit age distributions that is typically explained by a variety of natural factors such as differences in erosion rates (e.g., Amidon et al., 2005a), mineral fertility over the study area (e.g., Moecher and Samson, 2006; Dickinson, 2008), and fractionation by transport processes (e.g., hydraulic sorting) (Lawrence et al., 2011b; Malusà et al., 2016).

In detrital studies, minerals of interest such as zircon and apatite are more likely to be found in the 63–250 micron sand fraction. Inherent in these studies is the assumption that this fraction is representative of the system under investigation and that the upstream source units are homogeneously mixed. Lukens et al. (2016) showed that detrital methods focusing on a given size fraction (cosmogenic nuclides in sand in their case) could be biased in steep terrain, as some parts of the catchment may generate more sand than others (see also Riebe et al., 2015). Further, implicit in this practice (and by extension in sediment mixing models) is an untested assumption that pebbles with different abrasion rates are not able to statistically change (i.e., distort) the detrital age distribution of sands. However, fluvial abrasion of clasts has long been considered as one of the main drivers of mineral liberation from coarser to finer size fractions and thus one of the processes which, along with selective transport, promote downstream fining along a river (Krumbein, 1941; Kuenen, 1956; Schumm and Stevens, 1973; Mills, 1979; Parker, 1991; Attal and Lavé, 2006, 2009; Le Bouteiller et al., 2011; Domokos and Gibbons, 2012; Miller et al., 2014). The importance of abrasion in generating sand was confirmed by recent studies combining both field and laboratory investigations, (e.g., Sklar and Dietrich, 2001; Lewin and Brewer, 2002; Attal et al., 2006; Attal and Lavé, 2006, 2009).

Here, we investigate whether pebble abrasion can statistically change (distort) the detrital age distribution recorded by fluvial sands. The Marsyandi watershed, central Nepal, is an abrasion-dominant setting with exceptional constraints on the parameters that are required to simulate the evolution of sediment grain size and mineralogy: published U-Pb detrital zircon age distributions and zircon fertility datasets (Amidon et al., 2005a) are used together with pebble abrasion rates and hillslope grain size supply data (Attal and Lavé, 2006) to simulate detrital age distortions along the Marsyandi River. In addition, our model predictions are compared to other independent published datasets of sediment mixing (e.g., Garzanti et al., 2007) and erosion rates (e.g., Pratt-Sitaula et al., 2004; Gabet et al., 2008; Burbank et al., 2003) from the study area.

We initially test if, by using specific pebble abrasion rates, we are able to simulate statistically significant changes on the U-Pb detrital zircon grain age population from sands by comparing model results with and without abrasion. We also compare our no-abrasion model results with results from Amidon et al. (2005a)’s no-abrasion model as a test of our model’s performance. We then assess the magnitude of the distortion other well-known controlling factors (i.e., differences in erosion rates, zircon fertility and hillslope gravel supply) are able to generate in the Marsyandi catchment, and assess if abrasion is able to produce distortions of a

comparable magnitude. With these experiments, we test if pebble abrasion is a significant factor influencing the grains ultimately used in detrital studies, and the resultant grain age distributions used to investigate past landscape change.

2 Materials and Methods

2.1 Estimating the source mixing proportion in mixed sand samples

Measuring the U-Pb zircon grain age distribution both in upstream source units and in a downstream mixed river sample should be sufficient to obtain the mixing proportions of these source units by iteratively solving the proportions in which they must be present to produce a best fit (Amidon et al., 2005a,b).

The best-fit age distribution $f(x)$ of a downstream sample $g(x)$ derived from n source units is given as:

$$f(x) = \sum_{i=1}^n \Phi_i f_i(x), \quad (1)$$

where Φ_i is the zircon mixing proportion, equal to $1/n$ if all source rocks are equally represented, and must satisfy:

$$\sum_{i=1}^n \Phi_i = 1. \quad (2)$$

In Equation (1), $f_i(x)$ is the U-Pb zircon age distribution from the source unit i , and is mathematically represented by the probability density function (PDF):

$$f_i(x) = \frac{1}{\sigma_i \sqrt{2\pi}} e^{-\frac{1}{2} \left(\frac{x - \mu_i}{\sigma_i} \right)^2}, \quad (3)$$

where x is grain age, μ_i is the mean grain age and σ_i is the analytical uncertainty of the dating method (c.f. Saylor and Sundell, 2016).

The zircon mixing proportions Φ_i are iteratively estimated by minimizing the area mismatch (M) between the U-Pb zircon grain age distribution of the mixed sample $g(x)$ and the U-Pb zircon grain age best-fit $f(x)$ made of upstream source units $f_i(x)$. This minimization is performed by a mathematical optimization, which is solved in this work through the Sequential Least Squares Programming (SLSQP) method (Nocedal and Wright, 2000). Although PDF cross-plot maximization and Monte Carlo modelling seems to generate more accurate mixing proportions (Saylor et al., 2013; Sundell and Saylor, 2017; Sharman and Johnstone, 2017), we chose the area mismatch method to match the procedures adopted by Amidon et al. (2005a), as we are using their age populations and wish to produce results that are directly comparable with their no-abrasion model.

The area mismatch (M) accounts for discrepancies between the total area of two discretized PDFs (Amidon et al., 2005a) and can be calculated as:

$$M = \sum_{k=1}^n \frac{|f(x_k) - g(x_k)|}{2}, \quad (4)$$

where n represents the number of grain ages considered, x_1 and x_n represent the minimum and maximum ages, respectively, and $f(x_k)$ and $g(x_k)$ are the modelled and mixed sample age distributions, respectively.

We also use area mismatch (M) as a metric to analyze the age distributions predicted by the sediment mixing models (see section 2.4).

2.2 Mixing models

Both the abrasion and no-abrasion models that we apply in this work are 2D linear mixing models which predict fluvial sediment mixtures by a forward approach based on the characteristics of the zircons (i.e., age) and of the sediment sources units (e.g., fertility, exposure area and abrasion rate). Mixing models can also be used as inverse unmixing models to predict the erosion rates that match the age distributions and the best-fit fluvial sediment mixtures described in Equation 1. The theoretical and quantitative details of both models and how the mixing proportions and U-Pb detrital zircon grain ages are used are described below.

2.2.1 No-abrasion model

The no-abrasion model is a reproduction of the linear zircon (un)mixing model proposed by Amidon et al. (2005a). It predicts the mixing proportion of sands originating from upstream source units along any point on the river network. It is based on the exposure area and mineral fertility of the source units. In this model, the predicted zircon proportion Φ_i^P from a specific source i in a geological setting composed of n sources can be mathematically described as:

$$\Phi_i^P = \frac{A_i C_i}{\sum_{k=1}^n A_k C_k}, \quad (5)$$

where:

$$\sum_{k=1}^n A_k = 1, \quad (6)$$

$$\sum_{k=1}^n C_k = 1. \quad (7)$$

The predicted zircon mixing proportion (Φ_i^P), equal to $1/n$ if all source rocks are equally represented, must satisfy:

$$\sum_{i=1}^n \Phi_i^P = 1. \quad (8)$$

A_i and C_i refer, respectively, to relative exposure area and relative zircon concentration (fertility) of the source unit i . Multiplying the PDF of each source unit, $f_i(x)$, by its respective mixing proportion predicted by the model, Φ_i^P , allows us to create an artificial PDF, $h(x)$, corresponding to the age distribution expected for a case where pebble abrasion is not considered. The expression for $h(x)$ is similar to Equation (1) and can be written as:

$$h(x) = \sum_{i=1}^n \Phi_i^P f_i(x). \quad (9)$$

The discrepancies between predicted and best-fit mixing proportions estimated in subsection 2.1 (Φ_i^P and Φ_i , respectively) can then be attributed to different factors, including different relative erosion rates, Φ_i^R , for the different units (Amidon et al., 2005a) (e.g., a unit being eroded two times faster than other units will contribute twice the amount of zircon expected from the procedure above). These relative erosion rates, Φ_i^R , for the no-abrasion model can be iteratively estimated by:

$$\Phi_i = \frac{\Phi_i^P \Phi_i^R}{\sum_{k=1}^n \Phi_k^P \Phi_k^R}, \quad (10)$$

where Φ_i^R is equal to $1/n$ if all source rocks are eroded at the same rate and must satisfy:

$$\sum_{i=1}^n \Phi_i^R = 1. \quad (11)$$

They can also be estimated by minimizing the area mismatch, M , between the age distributions created by the model, $h(x)$, and the best-fit solution, $f(x)$.

2.2.2 Abrasion model

The abrasion model proposed in this work is also a linear (un)mixing model and its key assumptions are: (1) bedrock incision processes and downstream fining can be treated as steady state; (2) all particle sizes are moved downstream; (3) selective sorting as well as weathering are negligible on the considered timescale; (4) size reduction due to both breaking and attrition to sand is treated with a single abrasion rate; and (5) zircon proportion is homogeneously distributed in the generated sand fraction. Note that assumptions 1, 2, 3 and 5 are typically assumed in sediment mixing models. In this work, we also include assumption 4 because the abrasion experiments performed by Attal and Lavé (2006) do not discriminate abrasion products according to grain size (e.g., sand, silt, or gravel) and also because the abrasion rates they calculated encapsulate both breaking and attrition without distinguishing between these processes. The limitations imposed by our assumptions are discussed in section 4.4.

In the model, we assume each point across the catchment is a source of sediment belonging to a given rock unit i (see model implementation, section 2.3). The sediment supplied to the river system by each source is made of sand and clasts (“gravel”); we set the initial gravel mass fraction, F_{g0} , to 75 % in our reference runs, an average value for landslides in the Marsyandi valley (Attal and Lavé, 2006). We then record the distance d between each source point and a specific river site, and apply an empirically-defined version of the Sternberg’s law to calculate the proportion of the sediment initially supplied by the source unit that reaches the considered river site as gravel (F_g) (Dingle et al., 2017):

$$F_g = F_{g0} e^{-\alpha d} \quad (12)$$

According to Equation (12), the initial percentage of gravel mass F_{g0} changes to a percentage F_g at distance d from the origin, at a rate given by the rock unit-dependent abrasion rate α (in km^{-1}). The percentage of sand mass F_s at d is inversely proportional to the gravel mass F_g :

$$F_s = 1 - F_g \quad (13)$$

Note that the Sternberg’s law (Equation 12) as used in our work is a “generalized Sternberg’s law” that refers to mass loss and not to grain size fining (Miller et al., 2014). It is important to make this distinction because recent work by Domokos et al. (2014) and Miller et al. (2014) suggests that grain size fining due to abrasion does not follow the original Sternberg’s law: angular fragments initially experience a rounding phase during which mass is lost but grain size is not significantly reduced; once the grains have been rounded, both mass and grain size are reduced in concert. Their work suggests that mass loss described by Equation (12) applies to both abrasion phases, including the original rounding phase, and is therefore suitable to describe abrasion of fragments from their source, as in our model.

Given that every source unit i has a specific zircon concentration C_i (fertility), relative exposure area A_i and relative supply rate by erosion Φ_i^{ZR} , the zircon mixing proportion of the source unit i in river sands Φ_i^Z is given by:

$$\Phi_i^Z = F_s A_i C_i \Phi_i^{ZR} \quad (14)$$

at distance d .

Multiplying each single source unit PDF, $f_i(x)$, by the mixing proportion estimated by the model (Φ_i^Z) allows us to create an artificial PDF, $z(x)$, corresponding to the age distribution of a downstream sand sample as expected when abrasion does occur. The expression of $z(x)$ is similar to Equation (1):

$$z(x) = \sum_{i=1}^n \Phi_i^Z f_i(x). \quad (15)$$

As in the no-abrasion model, the relative erosion rates (Φ_i^{ZR}) can also be inversely estimated by minimizing the area mismatch (M) between the artificially created PDF, $z(x)$, and the best-fit sample age distribution, $f(x)$ (Fig. 1).

2.3 Model implementation

In our simulations, we use topographic data with ~ 90 m spatial resolution of the Marsyandi watershed from the Shuttle Radar Topography Mission (SRTM). From these elevation data, we define the river network (used to route sediment across the catchment) and extract flow length for each pixel across the watershed, using tools from the Geospatial Data Abstraction Library (GDAL). Flow length is used to calculate travel distance (km) from each pixel to a given river site (d in Equation 12). The source units (i in Equation 14) with their spatial extent [km^2] also feed the model as geographic layers. For a given “sampling” location along the river, each contributing pixel is assigned a transport distance d and a source unit i ; the relative exposure area of each unit A_i is calculated based on this information. For each source unit i , the initial percentage of gravel supplied by the hillslopes to the river channel (F_g), zircon concentration (C_i) and supply rate by erosion (Φ_i^{ZR}) are set by the user. After combining all those parameters and retrieving the zircon mixing proportion (Φ_i^Z) of every source unit for the river sands at the considered river site (Equation 14), we use Φ_i^Z as an input to create the artificial PDF ($z(x)$ in Equation 15). All the code used to perform our analysis as well as to

generate the figures is open source and can be downloaded from GitHub at <https://github.com/clavarini>.

2.4 Statistical analysis of model predictions

The PDFs constructed by the mixing models are statistically assessed by area mismatch (M), similarity coefficient (S), Kolmogorov–Smirnov test ($K-S$), PDF cross-plot analysis and Q-Q plots. The main aim of these analyses is to quantify how different the model predictions are by comparing their resulting age distributions based on specified scenarios.

Any statistically significant difference between the age distributions generated by the mixing models is hereafter named distortion.

2.4.1 Similarity coefficient (S)

The similarity coefficient S measures if samples have overlapping modes as well as similar proportions of components in each of the modes. Gehrels (2000) defines it as:

$$S = \sum_{k=1}^N \sqrt{f(x_k)g(x_k)} \quad (16)$$

where $f(x_k)$ and $g(x_k)$ are the probability density functions (PDFs) of samples one and two, respectively, and x_1 and x_N are the minimum and maximum ages for the population. An S value of 1 indicates that the PDFs are perfectly matched both in the modes and modal proportions, while a value of 0 indicates that the two age populations have no modes in common.

2.4.2 Kolmogorov–Smirnov ($K-S$) test

Traditionally, the Kolmogorov–Smirnov ($K-S$) test assesses the null hypothesis that two samples are drawn from parent populations with the same distribution. It calculates the $K-S$ statistic D_s , which is the maximum difference between the empirical cumulative distribution functions (CDFs) of the two analyzed samples, and returns a p -value that is inversely proportional to the confidence level at which the two samples fail the hypothesis. The D_s value is calculated as:

$$Ds_{1,2} = \sup_k |F_1(x_k) - F_2(x_k)|,$$

(17)

where $\sup(x)$ is the supremum of the set of distances, and F_1 and F_2 are the CDFs of the two samples made from n_1 and n_2 observations, respectively.

The probability p that the observed samples are from the same population was calculated by Stephens (1970) as:

$$p(Ds_{observed} > Ds_{critical}) = Q_{KS}(\lambda) = 2 \sum_{i=1}^{\infty} (-1)^{i-1} e^{-2i^2 \lambda^2} \quad (18)$$

where

$$\lambda = \left(\sqrt{n_e} + 0.12 + \frac{0.11}{\sqrt{n_e}} \right) Ds \quad (19)$$

and

$$n_e = \frac{n_1 n_2}{n_1 + n_2} \quad (20)$$

with limiting values of $Q_{KS}(0) = 1$ and $Q_{KS}(\infty) = 0$.

The K - S statistic represents a useful metric to investigate the similarity in the shape of detrital age distributions and to assess our artificially created PDFs. In cases where the distance Ds between the investigated PDFs approaches zero, p (or Q_{KS}) tends to 1, while extreme distances will tend to produce p values approaching 0. In this work, we retrieve both Ds and p values, since some studies have shown that in detrital geochronology Ds is more sensitive than its corresponding probability (p) (Satzoski et al., 2013; Vermeesch, 2013; Saylor and Sundell, 2016).

2.4.3 PDF cross-plot and quantile-quantile (Q-Q) plot

In statistics and probability, quantiles refer to specific cut points dividing the range of a probability distribution (PDF) into contiguous intervals with equal probabilities. A quantile-

quantile (Q-Q) plot is a plot where quantiles of two datasets are plotted against each other. In detrital studies, Q-Q plots are used to determine if two data sets come from populations with a common distribution. A PDF cross-plot is a Q-Q plot which, rather than using cumulative distribution functions (CDFs), is based on two PDFs (Saylor et al., 2012). The advantage of the cross-plot to examine detrital age distributions is that it is sensitive to the presence or absence of age peaks (e.g., Saylor et al., 2013). Samples with identical age peaks, peak shapes and peak magnitudes have $R^2 = 1$, while for those sharing no age peaks R^2 approaches 0. PDFs that share either some, but not all, peaks, or have peaks of different magnitudes or shapes, will produce cross-plots with R^2 ranging between 0 and 1.

2.5 Study area and experimental setting

2.5.1 The Marsyandi watershed

The Marsyandi watershed, in the central Himalaya, has an area of approximately 4700 km², is 57 km wide and 170 km long. The Marsyandi flows into the Trishuli River, which later joins the Ganga River in the Himalayan foreland basin. Elevation varies from 200 m to 8000 m. The sediment source units can be grouped into five litho-structural units (Le Fort, 1975; Amidon et al., 2005a; Attal and Lavé, 2006) (Fig. 2).

The uppermost source unit (Tethyan Series – “TTS”) comprises Cambrian to Jurassic limestones, sandstones and shales. The Tethyan Series are intruded by a Miocene leucocratic granite (Manaslu granite – “MG”) in its eastern section. The southern margin of the Tethyan Series is marked by a north-dipping, normal-sense shear zone known as the South Tibetan Detachment (STD). Below (south of) the STD lies the Greater Himalayan Series (GHS), a continuous sequence of amphibolite-grade schists and gneisses divided from south to north into three formations, grouped here as pelitic gneisses (Formation I – “FI”) and Paleozoic augen gneiss intrusions in calc-silicate rocks (Formation II-III – “FII-III”) (Le Fort, 1975). The series are in turn bounded to the south by the Main Central Thrust (MCT). The MCT is the structural boundary between the Greater Himalaya and Lesser Himalaya series. Lower-grade schists and meta-sediments of the Lesser Himalayan Series (“LH”) occur in the MCT footwall.

2.5.2. The Marsyandi dataset

In our study case, we test the effects of abrasion on detrital information using the Marsyandi catchment as a template. The mixing proportion of sands, pebble abrasion rates and zircon fertility of the source units are derived from Attal and Lavé (2006) and Amidon et al.

(2005a). The abrasion rates for rock types (e.g., sandstone, schist, etc.) of Attal and Lavé (2006) (their Table 2) are converted to a representative value for the source units of Amidon et al. (2005a) by applying weighted arithmetic mean corrections (Table 1). The U-Pb detrital zircon grain ages are from Amidon et al. (2005a) (Supporting Information Table S1); age smoothing was applied prior to statistical analysis with the same age window interval (80 Ma) as used by Amidon et al. (2005a). We also performed statistical comparison (i.e., S , M , PDF cross-plot, Q-Q plot, and $K-S$ statistics) between age distributions with and without smoothing to test if statistically significant changes occur and, therefore, biases the sediment (un)mixing results. Our statistical comparison are in the Supporting Information (Tables S3 and S4) and are discussed in a section dedicated to methodological uncertainties (4.4).

Shuttle Radar Topography Mission (SRTM) elevation data with ~90 m of spatial resolution are used as topographic data in the mixing models. The modelling calculations are performed for three river locations where samples were collected (Fig. 2). The uppermost sampling point (E) has three contributing source units (TTS, MG and FII-III); the sampling point (G) has four (TTS, MG, FII-III and FI), and the Marsyandi outlet (K) has all five. Numerical tests of the minimizations were performed to solve for the relative erosion rates (presented in section 3).

2.5.3 Experimental setting

In all numerical experiments where we test for factors controlling zircon mixing, we use synthetic U-Pb age distributions for the sources in addition to the natural age distributions of Amidon et al. (2005a). The synthetic distributions are normal, with specific age peaks (μ) of 0.5, 0.8, 1 and 1.2 Ga for the Tethyan, Formation II-III, Formation I and Lesser Himalaya sequences, respectively, and a standard deviation (σ) of 5 % (Fig. 2, Equation 3, Supporting information Table S2). This spread of age is comparable to the spread in the real dataset. We adopted ages increasing downstream so that the relative contribution of the different sources is easier to identify in the mixed sample distributions; we also chose to have a distinct peak (Tethyan Series at 0.5 Ga) and three partly overlapping distributions, comparable to the real dataset. We performed additional experiments with four additional synthetic age distributions with various degrees of peak overlap to assess the influence of this factor (discussed hereafter and presented in the Supporting Information).

2.5.3.1 Testing the influence of abrasion rates on age distributions

In our first set of simulations, we test the influence of pebble abrasion rates on mixed sample age distributions (scenarios A1–A4). Zircon fertility is the same for all sources, except for the Manaslu granite for which zircon fertility is set to zero to reproduce the behaviour of a non-contributing source region to the age distribution, as Amidon et al. (2005a) found no zircon within the Marsyandi watershed that they could unambiguously relate to the Manaslu granite. The hillslope gravel supply is also set to a uniform value of 75 %. The abrasion rates used in the simulations are based on experimental abrasion rates for rock types of the Marsyandi watershed from Attal and Lavé (2006) (Table 2).

In the first scenario (A1), the effect of uniform abrasion is assessed by setting a single abrasion rate of 0.4 %/km, (equivalent to granite) for the whole watershed. In the second scenario (A2), we simulate the behaviour of a watershed with two extreme rock strengths: rocks from the Tethyan Series have a high abrasion rate of 31 %/km, (equivalent to poorly cemented sandstone) and the rest of the rocks are abraded at a low rate of 0.15 %/km (equivalent to quartzite). In the third experiment (A3), we assess how source location impacts fluvial sand composition by inverting the previous scenario: the Lesser Himalaya has the highest abrasion rate (31 %/km) while rocks from the upstream sources are abraded at 0.15 %/km. In the fourth scenario (A4), we apply abrasion rates representative of the different units in the Marsyandi watershed (Attal and Lavé, 2006). The main aim of this experiment is to simulate how the fluvial sand composition behaves in a complex scenario of rocks with multiple abrasion rates but decoupling it from other controlling factors that can bias the sand mixing proportion.

2.5.3.2 Comparing the influence of different controlling factors on age distributions

In a second series of experiments, we test the sensitivity of the age distributions to abrasion rate (B2), erosion rate (B3), fertility (B4), and initial gravel fraction (B5). The experiments are run using both synthetic and natural datasets. The parameter values used to create the scenarios are chosen to emphasise the distortion in sand while keeping within a realistic range. Variations in erosion rate, abrasion rate, hillslope gravel supply and zircon fertility are applied based on values published by Garzanti et al. (2007), Attal and Lavé (2006) and Amidon et al. (2005a), respectively (Table 3). Scenario B1 is the reference scenario with all parameters spatially uniform and no abrasion (see Fig. 3, “no abrasion”). In scenario B2, abrasion rate for Tethyan Series gravel varies between 0.15 and 31 %/km while it is kept at 0.15 %/km for the other units; the experiment with the most extreme value (31 %/km) is the same as A2. In B3, the Tethyan Series are eroded between 1 and 5.1 times faster than the rest of the

catchment. In B4, the fertility of rocks from the Tethyan Series is 0.8 grains/g while it is set to between 0 and 0.8 grains/g in the rest of the catchment; the experiment where all non-TTS units contributes no zircon (fertility = 0) simulates an extreme scenario with “invisible” units. In B5, sediment initially sourced from the Tethyan Series is made of between 60 and 90 % of gravel (i.e., between 10 and 40 % sand) while this number is 90 % in the rest of the catchment; this range of values encompasses values from landslides in different lithologies measured in the Marsyandi valley (Attal and Lavé, 2006). Scenario B5b is the same as B5, except that the initial gravel fraction varies between 60 and 90 % for the Lesser Himalaya sources (instead of TTS) while this number is 90 % in the rest of the catchment; this scenario tests the influence of peak overlap, as the LH peak in the synthetic dataset overlaps with the Formation I peak (see next section). Finally, we explore a scenario where Tethyan Series have both an extremely high abrasion rate (31 %/km) and the lowest initial gravel fraction (60 %) supplied to the river channel, while the other source units have low abrasion rates (0.15 %/km) and hillslopes with an extremely high gravel content (90 %) (scenario B6). The aim of this experiment is to test the influence of the known covariance between highly abradable source units and higher sand supply from hillslopes due to higher weathering rates in softer rocks (e.g., schist versus quartzite, see Attal and Lavé, 2006).

2.5.3.3 Testing the ability of controlling factors to reproduce the distortion from others

In these experiments, we test how well each controlling factor can mimic the distortion caused by another factor in the most extreme scenarios from experiments B2 to B5, using both synthetic and natural datasets. We use the maximum and minimum values used in the experiments B2 to B5 as bounds to iteratively solve for the best fit between the age distribution created from a factor being tested and a factor whose distortion is intended to be reproduced.

To test the ability of the method to cope with relative changes in partly overlapping age peaks, we explore a scenario where the Lesser Himalaya has the smallest gravel fraction (60 %) instead of the Tethyan Series (scenario B5b instead of B5, see Table 3) as the LH peak in the synthetic dataset overlaps with the Formation I peak (whereas the TTS peak is isolated).

2.5.3.4 Testing the influence of abrasion on mixing proportions in the Marsyandi catchment

Finally, we use the Marsyandi dataset to assess the influence of abrasion on both mixing proportions and age distributions in a real scenario, using the parameters described in Table 1.

For the three mixed samples E, G and K (Fig. 2), we compare best-fit results using the iterative method described in section 2.1 with the results obtained from the mixing models with and without abrasion. At each site, we discuss the differences and their statistical significance.

3 Results

3.1 Simulations for sensitivity analysis

3.1.1 Influence of abrasion rates on age distributions

Simulations A1 to A4 demonstrate how pebble abrasion affects the zircon mixing proportions of upstream sediment source units in the sand fraction and ultimately distorts the grain age distributions (PDPs) of the mixed samples derived from them (Fig. 3). Modifications in the zircon mixing proportions (Fig. 3a) and in the shape of the PDPs are recorded in all experiments but not all of them are significant (Fig. 3c, e). The experiments that simulate extreme contrast in abrasion rates (A2 and A3) have changes in the zircon mixing proportion that distort all U-Pb grain age distributions investigated (see the R^2 values of the PDF cross-plots). Extremely high abrasion rates (31 %/km versus 0.15 %/km) lead to rapid release of zircon from gravel to sand for the unit in question. The unit therefore ends up overly represented in the mixed sand sample: more than 50 % of the zircons in the mixed sample are sourced from TTS and LH in scenarios A2 and A3, respectively (Fig. 3a). In the synthetic datasets (Fig. 3b), this is shown by the clear growth of the TTS and LH source peaks, respectively.

The trends with the natural datasets are less clear, as peaks are not as well defined, overlap, and do not have a normal distribution; units are not characterised by a single peak neither (Fig. 2). All scenarios (A1-A4) show significant statistical changes in the age distributions, overall greater than with the synthetic datasets (Fig. 3d, e). The only exception is scenario A2, in which more distortion is observed with the synthetic dataset (Fig. 3c, e). This can be explained by the fact that TTS shares its major peaks (in range 0.5-1 Ga) with Formations I, II and III (Fig. 2): a relative increase in zircons from TTS in the range 0.5-1 Ga due to rapid abrasion is counterbalanced by a relative decrease in zircons from Formations I, II and III in the same age range. On the other hand, the dominant age peak from LH at ~1.8 Ga is unique, leading to the greatest amount of distortion ($R^2 = 0.69$, Fig. 3e) and a clear growth of this peak in experiment A3 (Fig. 3d).

Interestingly, numerical changes in the zircon mixing proportions and age distributions in the uniform abrasion scenario (A1) are comparable to when abrasion reflects the real variations of the rocks from the Marsyandi watershed (A4), both with synthetic and natural

datasets. Statistically, however, in both cases (A1 and A4), the K - S tests and PDF cross-plots are not able to demonstrate that these populations are different from a no-abrasion scenario (with 95 % confidence) and therefore no statistically significant change (distortion) is identified. The similarity coefficient (S) and Q-Q plot statistics are less sensitive in detecting changes in the grain age distributions but also mirror the trends identified by the PDF cross-plots and area mismatch (M) (Supporting Information Table S5-S6 and Fig. S2). Finally, additional experiments with synthetic datasets characterised by peaks with various shapes and degrees of overlap provide very similar results overall (Supporting Information Fig. S1, S2 and Table S11): R^2 values for experiments A1 and A4 are barely affected by the changes (changes are within 5 %) and experiments A2 and A3 generate the greatest amount of distortion. However, the isolation and broadness of the peak targeted by the change in abrasion rate seem to affect the relative amount of distortion in scenarios A2 and A3: A3 generates greater distortion than A2 when peaks are well isolated (age distributions 1 and 2), and the opposite when there is significant overlap (age distributions 3-5). This demonstrates a sensitivity of the results to the shape of the age distributions, though the R^2 values for experiments A2 and A3 tend to be very close, no more than 16 % from each other.

3.1.2 Influence of the different controlling factors on age distributions

We produced age populations in a range of scenarios, whereby the Tethyan Series are assigned distinct values from all other units for abrasion rate, erosion rate, zircon fertility and gravel fraction in sediment supply (scenarios B2, B3, B4 and B5, respectively; Table 3). The results are populations where the peak at 0.5 Ga is enhanced with respect to the other peaks (Fig. 4a-d). The experiments highlight that all of these controlling factors affect the zircon mixing proportions and statistically distort the age distribution of modern river sands. The response is linear for erosion rate, fertility and initial gravel fraction (e.g., a doubling of erosion rate in the TTS units leads to twice more zircon from this unit); the response is strongly non-linear with respect to abrasion rates, with high sensitivity at low abrasion rates and no sensitivity at rates above 2 %/km (Fig. 4a). When combining both high abrasion rate and high initial sand content at the source (scenario B6), we observe increased distortion compared to scenarios with either high abrasion rate or high initial sand content at the source (Fig. 4f): the TTS unit is overrepresented in the sand sample due to a relatively greater proportion of zircons from other units being “retained” in gravel, as a comparatively greater amount of gravel from these units is supplied at the source and this gravel persists for longer (lower abrasion rate).

We find that, within the realistic range of values for the Marsyandi catchment, the factors that can produce the highest distortion are, from highest to lowest: fertility, erosion, hillslope gravel supply and, lastly, pebble abrasion (Fig. 5). This order is valid for both synthetic and natural datasets, though the amount of distortion in the natural dataset tends to be lower, possibly due again to the fact that TTS shares peaks with other units (Fig. 5). We note that increasing peak overlap in the synthetic datasets leads to a systematic increase in distortion (lower R^2 values in PDF cross-plots) for all scenarios (Supporting Information Fig. S3 and Table S11).

As in the previous section (3.1.1), metrics such as the similarity coefficient (S) and Q-Q plot statistics are the least sensitive to detecting changes in the grain age distributions but mirror the trends identified using the PDF cross-plots and area mismatch (M) (Supporting Information Table S7, S8 and Figure S3, S4).

3.1.3 Ability of controlling factors to reproduce the distortion from others

We assess the capability of different distorting factors to reproduce the distortion created in experiments B2–B6. We use the optimization method to assess whether, for example, the age distribution produced by scenario B2 (Tethyan Series rocks abraded at 31 %/km) can be mimicked by allowing other parameters (relative erosion rates, fertility and gravel supply) to vary, in turn, within the range of realistic values (Fig. 6, see also experiments with different synthetic datasets in Supporting Information Fig. S5).

We find that all the factors are able to perfectly reproduce the impact of abrasion on the zircon grain age distribution (B2) (Fig. 6; statistics in Supporting Information Table S9, S10). The effect of having Tethyan Series rocks abraded at 31 %/km while the others are abraded at 0.15 %/km can be replicated by having the Tethyan Series' erosion rate, fertility or initial sand supply ($= 1 - \text{initial gravel supply}$) around three times greater than that of the other units (Supporting Information Table S13). On the contrary, abrasion is not able to fully reproduce the distortions caused by any other controlling factor (Fig. 6). Changes in fertility are able to fully reproduce the distortion caused by differences in relative erosion rates (B3 – erosion of Tethyan Series five time faster than other units), but changes in abrasion rates or gravel fraction can produce distributions similar enough (not statistically distinct; Fig. 6). No factor can fully reproduce the distortion caused by extreme differences in fertility (B4); this occurs as a result of having three “invisible lithologies” with fertility = 0. Any lithology containing zircons will appear in the mixed sand sample, irrespective of their abrasion rate, initial gravel fraction or

relative erosion rate (except in an unimaginable scenario where erosion rate = 0 or gravel supply = 100 % and abrasion rate = 0). All factors except abrasion are able to reproduce the age distribution resulting from variation in hillslope gravel supply, even in a situation where the peak that is affected (i.e. Lesser Himalaya) partly overlaps with other peaks (scenario B5b, Table 3, Fig. 6). These results apply to both synthetic and natural datasets (Fig. 6).

It is interesting to note that in all cases, abrasion produces peaks that are not high enough to replicate the extreme distortion caused by the other factors. In other words, not enough sand is produced by abrasion from the Tethyan Series in experiments B3 and B4 and from the Lesser Himalaya in experiment B5b. This results from abrasion rates being allowed to vary only between 0.15 and 31 %/km. When looking at the statistics of the results, however, we find that the “best fit” is given for abrasion rates of 3.5 and 3.3 %/km for the Tethyan Series for experiments B3 and B4, respectively, while the other lithologies are being abraded at 0.15 %/km (Table S6). This is unexpected as, in theory, more sand from the Tethyan Series could be generated with greater abrasion rates (up to 31 %/km). This occurs as a result of the termination threshold in the minimization procedure in the model, as iterations stop when the minimization does not reduce the misfit by more than 0.1 % in the cost function. In case B3, for example, we find that the proportions of zircon sourced from the Tethyan Series are 52.48 % and 52.54 % with abrasion rates of 3.5 and 31 %/km, respectively: mixing proportions are insensitive to abrasion rates beyond a given value, as shown in the sensitivity analysis (Fig. 4a). On the other hand, the best-fit abrasion rates in scenario B5b are 30.3 %/km for the Lesser Himalaya and 0.15 %/km for the other lithologies: in this case, the proximity of the Lesser Himalaya units to the outlet makes the mixing proportions more sensitive to changes in abrasion rates for these units. These results highlight the non-linear dependency of mixing proportions on abrasion rates, as opposed to the other factors (a doubling of fertility in one unit can be mimicked by a doubling of relative erosion rate for this unit). They also demonstrate the effectiveness, and limitations, of the optimization method.

3.2 Study case (Marsyandi watershed)

In this last section of the analysis, we consider the real datasets to assess the importance of abrasion in controlling the age distribution of mixed samples and the relative erosion rates retrieved from them. In the following, we mix the real source age distributions to match the mixed sample age distributions measured in locations E, G and K (Fig. 2). We first produce a best-fit mixed sample distribution using the mismatch minimization method described in

section 2.1 and used in section 3.1.2. We then use our full mixing models (abrasion and no-abrasion, see section 2.2) that include field-derived parameters (Table 1) to attempt to replicate the best-fit distributions and retrieve relative erosion rates for the different units that make up the Marsyandi watershed. As mentioned earlier, the minimization method is an iterative procedure that stops when the iteration does not reduce the misfit by more than 0.1 % in the cost function. The cost function we use to produce the best-fit mixed sample distribution is the ratio of predicted to measured sums of squares of zircon ages (see section 2.1). The cost function we use for the full mixing models is area mismatch, to follow the procedure by Amidon et al. (2005a). Results for this section for the three sampling sites (E, G and K) are presented in figures 7, 8 and 9, respectively (see also Supporting Information S14, S15, and S16). We find that the grain age distributions created with the abrasion and no-abrasion models are statistically indistinguishable in all river reaches analyzed. However, the zircon mixing proportions and the relative erosion rates estimated from the same ages are different.

In the uppermost sampling site (E), only two sources are contributing (Tethyan Series and Formation II-III). When trying to best fit the no-abrasion and abrasion models (Fig. 7), we find a difference of 6 % between the zircon mixing proportions estimated by the two models (Fig. 7a). In spite of this, the modelled ages have an indistinguishable distribution ($R^2 = 0.988$). However, the relative erosion rates derived from these two models are significantly different: the relative contribution of the FII-III rises from 58.3 to 71.3 % when abrasion is accounted for, to counterbalance the increased zircon contribution from the Tethyan Series due to its relatively high abrasion rates (4.3 %/km, compared to 0.4 %/km for FII-III) (Fig. 7). The strong contrast in rock resistance to abrasion in this case (an order of magnitude) leads to a strong difference in predicted relative erosion rates.

At the intermediate site (G), the influence of abrasion is mostly visible in the proportions of Tethyan Series and FI: the abrasion model predicts that the Tethyan Series contributes 12 % more zircon at the sampling site than the no-abrasion model (65 instead of 53 %), while the contribution of FI is reduced from 28 to 16 % (Fig. 8a). This may be the result of the two units sharing part of their peaks in their age distributions (Fig. 2). Interestingly, this change is accommodated by relative erosion rates with an opposite trend, as Tethyan Series rocks are the most erodible and thus release more sand (and zircons) as they are transported further downstream: relative erosion rate of FI increases from 25.6 to 39.3 % while it drops from 40 to 29.3 % for the Tethyan Series. All modelled distributions are statistically indistinguishable from each other (Fig. 8b, c).

At the outlet sampling site (K), the results are not consistent with results from previous sampling sites (Fig. 9). Firstly, the best-fit distribution predicts zircon mixing proportions that are significantly different from those derived from the no-abrasion and abrasion models: the mixing models (both abrasion and no-abrasion) predict a much lower contribution from Tethyan Series and Lesser Himalaya (by up to 10 % each) and a much greater contribution from FI (by 15–20 %). This highlights the non-uniqueness of the solutions and the sensitivity to the approach used, in particular when sources have distributions that partly overlap (Fig. 2). Secondly, the relative erosion rates predicted for the abrasion and no-abrasion scenarios are very similar, despite the significant differences at the sites upstream: differences in relative erosion rates for each unit do not exceed 2.2 % (Fig. 9a) and the distributions produced are nearly identical (Fig. 9b, c). In some circumstances, overlap of the distributions and spatial differences in abrasion rates may conspire to compensate for abrasion and erosion effects, leading to a limited influence on the inversion outcomes.

4 Discussion

4.1 Abrasion as a distorting factor

Our numerical simulations using empirically-derived abrasion rates agree with recent research that highlights grain size biasing as one of the factors controlling the mineralogy and, therefore, the grain information of sands transported by rivers (e.g., Aguilar et al., 2014; Codilean et al., 2014; Carretier et al., 2015). The importance of abrasion in distorting grain age distributions is, however, more debatable. Although changes in the zircon mixing proportion can occur in watersheds of homogeneous lithology (e.g, experiment A1) and of diverse abrasion rates (e.g., A4), the resulting age distributions may not appear significantly distorted. Recently, Saylor and Sundell (2016) highlighted the limitations in the current statistical methods to assess changes in PDFs and, earlier, Vermeesch (2012) discussed the low sensitivity of PDPs to changes in zircon proportions. In both cases, there is supporting evidence explaining why numerical changes in the zircon mixing proportions are not necessarily followed by distortions of the age distribution statistics.

However, in watersheds of very different rock strengths (e.g., experiments A2 and A3, and sampling site E in the Marsyandi watershed), the distortions caused by abrasion are unambiguous. These findings highlight that sources of different rock strengths such as quartzite and sandstone found in complex tectonic environments (e.g., pro- and retro-foreland basins) can have their detrital age signatures significantly changed in modern river sands. Moreover, distorted grain age distributions within sediment reaching continental platforms can be

preserved in siliciclastic rocks and in the product of their recycling (e.g., metamorphic rocks) (Campbell et al., 2005; Perez and Horton, 2014; Sharman and Johnstone, 2017). Therefore, recognizing these distortions is important to more accurately (un)mix grain age distributions through modelling and inform provenance analysis from sedimentary archives.

The circumstances under which bias from abrasion is expected to be significant are summarised in Fig. 10. Even in the absence of contrasts in rock resistance to abrasion, bias will be expected if transport distance is short relative to abrasion rate (Fig. 10a, b). As sediment is transported downstream, the relative proportion of remaining gravel (and therefore “trapped” zircon) decreases downstream: in catchments where sediment has been transported over long distances, most of the gravel is turned into sand and most zircons have therefore been released in the sand fraction, limiting bias (Attal and Lavé, 2006, 2009; Dingle et al., 2017). What defines “long” or “short” distances is the abrasion rate (Fig. 10b): in a simple model where sediment is constantly supplied along a linear river system and gravel is abraded at a given rate (Attal and Lavé, 2006, 2009), we can calculate the amount of gravel that has been turned into sand at a given distance downstream. For very erodible gravel abrading at 20 %/km, more than 60 % of all gravel that has been supplied to the river has been turned into sand 10 km downstream from the river origin: we can therefore expect limited bias after distances in the order of 10-20 km. For gravel abrading at 2 %/km, this figure is 10 %: a significant amount of zircon remains “trapped” within gravel. The result is shown in Fig. 1b: at a point 20 km downstream of a river system made of half a lithology 1 and half a lithology 2, we find that 72 % of the sand sampled comes from the lithology exposed in the top half of the catchment due to greater transport distance, despite the fact that the river has been supplied the same amount of sediment from both units and that gravel from both units is abraded at the same rate of 2 %/km. For lithologies abrading at such rate, we expect limited bias after transport distance of the order of 100-200 km (Fig. 10a, b; Attal and Lavé, 2006, 2009; Dingle et al., 2017). Finally, gravel from resistant rocks (abrasion rate ≤ 0.2 %/km, e.g. quartzite, volcanics, mica-poor gneiss or granite, see Attal and Lavé, 2009) will persist for distances in excess of 1000 km (Fig. 10b): a significant amount of zircon from these units is therefore likely to remain trapped in gravel even in very large, continental-scale catchments, leading to their underrepresentation in sand samples. This is why strong contrasts in rock resistance to erosion and the presence of hard rocks will lead to bias from abrasion, irrespective of catchment size (Fig. 10a).

4.2 Influence of abrasion versus other factors

According to our simulations, abrasion is one of the factors with the lowest capability of distorting the detrital age distribution of sands among all currently considered controlling factors. Based on the Marsyandi's natural datasets, all considered factors are able to reproduce the distortion caused by abrasion in the age distribution, which may explain why abrasion has long been stated as a factor of minor influence in detrital geochronology (e.g., Malusà et al., 2013). Unlike abrasion, the other parameters tested have a linear relationship with the mixing proportions: for example, a doubling of erosion rate or fertility from one unit will lead to a doubling of the zircon contribution from this unit in a mixed sand sample further downstream. This is in stark contrast with our result showing that the effect of having Tethyan Series rocks abraded at 31 %/km while the other lithologies are abraded at 0.15 %/km can be replicated by having the Tethyan Series' erosion rate, fertility or initial sand supply (the converse of gravel supply in our study) around three times greater than that of the other units (Table S5 and S6). It is important to note, however, that this number is strongly controlled by the initial gravel (or sand) supply: in our reference scenarios, the initial sand supply is set to 25 % for all units. As a result, total abrasion of Tethyan Series gravel into sand (due to an extremely high abrasion rate) will lead to an extra 75 % of sand at the outlet, that is, a quadrupling of the amount of sand sourced from the Tethyan Series (compared to a scenario with no abrasion). This would lead to zircons from the Tethyan Series being four times more abundant in our mixed sample, if gravel from other lithologies were not abraded. We found Tethyan Series zircons around thrice more abundant in our scenario (experiment B2, Table S13), due to gravel from other lithologies being abraded. The initial gravel fraction therefore puts an upper limit on the amount of distortion that can be generated through abrasion when strong differences in abrasion rates exist. Initial gravel supply of 90% could potentially generate abrasion-driven differences in mixing proportions of up to an order of magnitude, as discussed below.

Zircon fertility is a highly variable parameter, with some units potentially being devoid of zircon and therefore being invisible in subsequent mineral selective dating. In our simulations, zircon fertility of the source units has the largest control on grain age distortion. Recent research on terrains of varied zircon fertility suggests that fertility is the main driver of natural bias in detrital geochronology, and that constraining this bias is an essential step in improving the reliability of dating techniques (Moecher and Samson, 2006; Glotzbach et al., 2017).

In our study, we vary hillslope gravel supply between 60 and 90 %, so sand supply varies within a factor of ~4, between 10 and 40 %. Whereas sources of sediment may have

gravel supplies beyond these bounds (e.g., glacial sediment can have up to 70 % of its volume made of particles finer than 1 mm), we believe that this range is representative of most sediment sources in active mountain ranges (e.g., Attal and Lavé, 2006). Confirming this point, Casagli et al. (2003) measured grain size for 42 landslide dams in the Northern Apennines, Italy, and found that ~90 % of the studied deposits had a “gravel” fraction (> 2 mm) making up between 60 and 90 % of their volume. The lower potential variability in gravel supply compared to fertility limits the potential bias created by variations in this parameter. In addition, these variations will be irrelevant if the source units are abraded rapidly and/or if transport distance to the sampling point is long, as in these cases most of the gravel will have been turned into sand by the time it reaches the sampling point (Dingle et al., 2017). It is important however to recognize gravel supply as a potential source of bias for catchments with strong contrasts in gravel abrasion rates and/or short catchments, as illustrated in the following experiments (Fig. 10c).

Here, we use again the simple linear model of sediment supply and abrasion (Attal and Lavé, 2006, 2009) to calculate the amount of sand coming from the abrasion of gravel as a function of distance downstream, initial gravel supply and abrasion rate (Fig. 10c). Initial gravel supply controls the maximum amount of sand that can be released by abrasion (and therefore create bias), whereas abrasion rate dictates how quickly this sand is produced. If the initial sand supply (the converse of gravel supply) is low, then most sand will come from abrasion, leading to greater potential for bias. If the initial sand supply is high, then most of the sand in the river will originate from the source rather than from abrasion, at least in the upper part of the catchment (short transport distance = low amount of zircon released by abrasion); differences in relative zircon proportions from different lithologies will therefore more likely reflect differences in initial sand supply between the lithologies. We consider a point 50 km downstream from the river origin (Fig. 10c): if the lithologies exposed in the catchment are abrading at 20 %/km, then most of the gravel (> 90 %, see Fig. 10b) will have been turned into sand so there will be no bias from abrasion, whatever the initial gravel fraction is. If the lithologies exposed in the catchment are abrading at 0.2 %/km, then most of the sand will have originated from the initial supply (e.g., > 90 % of the sand if the initial gravel supply is 60 %, Fig. 10c); in this case, difference in relative zircon proportions will reflect differences in initial gravel supply (e.g., if one lithology has an initial 40 % sand fraction and the other 10 %, then there will be four times more sand from the former in the mixed sample, all else equal). The trade-offs between initial gravel supply and abrasion rate are not entirely intuitive and certainly

require further work; however, the model highlights again the strong potential for bias by abrasion in the presence of highly resistant rocks.

4.3 Abrasion and erosion in the Marsyandi region

Inverse modelling of sediment grain age distributions in the Marsyandi River using our mixing models reveals that the estimated relative erosion rates are highly sensitive to abrasion, despite the amount of grain age distortion not necessarily being statistically significant. For the sampling site E (upstream), calculated erosion rates are in rough agreement with those estimated by other studies (e.g., Burbank et al., 2003; Pratt-Sitaula et al., 2004; Garzanti et al., 2007; Gabet et al., 2008). For instance, Garzanti et al. (2007) found relative erosion rates of 22.5 % for Tethyan Series and 77.5 % for Formation II-III, against 29 % for Tethyan Series and 71 % for Formation II-III from our abrasion model (Fig. 7). The no-abrasion model yields distinct relative erosion rates, with 42 % and 58 % for the Tethyan Series and Formation II-III, respectively.

At sampling site G (intermediate), our relative erosion rates are again in good agreement with published research which tends to show a downstream increase in erosion rates (Fig. 8). For instance, when converted to relative erosion, Garzanti et al. (2007) found relative erosion rates of 10 %, 34 % and 56 %, while our abrasion model suggests 29 %, 32 % and 39 % for the Tethyan Series, Formation II-III and Formation I, respectively. The relative erosion rates estimated by the no-abrasion model suggest an upstream increase in relative erosion rates, with rates varying from 26 % (Formation I) to 40 % (Tethyan Series). Modern erosion rates in the Himalaya suggest a spatial correlation between precipitation gradients and erosion that is enhanced by the tectonic uplift of the MCT hanging-wall (Hodges et al., 2004; Deal et al., 2017; Olen et al., 2015). Our modelling suggests that abrasion is also important as the no-abrasion model predicts different trends.

At the Marsyandi outlet (K), differences in relative erosion rates for each unit do not exceed 2.2 % and the distributions produced by the abrasion and no-abrasion models are nearly identical (Fig. 9). The abrasion model predicts relative erosion rates ~2 % greater for Formation I, but the difference is too small to be attributed it to any specific factor. Such a result would be expected if all gravel had been turned into sand, as in this case the mixing proportions would mimic a no-abrasion scenario. The transport distance over which around 90 % of the initial gravel is turned into sand by abrasion can be calculated as $250/\alpha$, where α is the abrasion rate in % mass loss / km (Equation (12)) (Attal and Lavé, 2006; Dingle et al., 2017). Based on the

abrasion rates used in this study (Table 1), this distance is 58, 625, 179 and 27 km for the Tethyan Series, Formation II-III, Formation I and Lesser Himalaya, respectively. Tethyan Series gravels will have travelled at least 130 km (Fig. 2) so very few of them would have survived to the outlet (site K). Formation I sediment will have travelled between 70 and 120 km so we expect no more than a quarter of it to have reached site K as gravel. Lesser Himalaya units are exposed closest to the outlet but their high abrasion rate (9.4 %/km) means that a large part of the sediment derived from it will also reach site K as sand (the distance between MCT and site K is 80 km, see Fig. 2). However, transport distances for the resistant Formation II-III range between 100 and 140 km, meaning that between 40 and 50 % of the sediment sourced from this unit should reach site K as gravel. This should lead to a strong underrepresentation of the Formation II-III in the mixed sand sample and therefore greater calculated erosion rates to counterbalance this effect, which we do not observe. We hypothesize that this is a coincidence potentially resulting from overlapping source age distributions (e.g., shared peak at ~0.5 Ga in Tethyan Series and Formation II-III, see Fig. 2): in some circumstances, this overlap combined with spatial differences in abrasion rates may compensate for abrasion and erosion effects, leading to a limited influence on the inversion outcomes. In general however, we expect the effect of abrasion on mixing proportions to decrease with increasing transport distance in the absence of very strong lithologies.

Overall, with the exception of sampling site K, our predictions of relative erosion rates using an abrasion model are better correlated with documented rates and spatial variability found by other studies. Pebble abrasion, based on lithology, can therefore be an important factor to consider when inversely solving for modern erosion rates.

4.4 Methodological uncertainties and limitations

Inverse modelling to predict erosion rates is known to be difficult and subject to model specifications as well as uncertainties in grain age distributions. There is no consensus on how to choose statistical analyses to (un)mixing age distributions (Saylor and Sundell, 2016). In our case, we worked with area mismatch (M) to be able to compare our results directly with those from Amidon et al. (2005a). However, this metric is known to have limitations when used to unravel grain age distributions (Sundell and Saylor, 2017) and may not be the most sensitive method to identify the influence of abrasion rates in detrital grain age signatures. Furthermore, working with unique solutions of mixing proportions can be problematic (Saylor and Sundell, 2016; Sundell and Saylor, 2017; Sharman and Johnstone, 2017), since small variations in

854 mixing proportions may produce statistically similar (and fitting) distributions but significantly
855 impact the results of inverse erosion modelling (e.g., relative erosion rates). These issues can
856 be dramatically enhanced when smoothing the age distributions (see Supporting Information
857 Tables S3 and S4). In the natural age distributions (samples E, G and K), the smoothing
858 procedure produces statistically significant changes in two samples (TTS and mixed sample,
859 K). Additionally, by reducing age variability, it favours convergence when finding mixing
860 proportions from source units (Amidon et al., 2005a). These differences in the sensitivity of the
861 (un)mixing techniques can obscure detectable variations in the age distributions caused by
862 pebble abrasion.

863 Another important consideration is the effect of intrinsic characteristics of age
864 distributions (i.e., the ages and their relative probability) in statistical analyses. Our experiments
865 with different age peaks show that the ability of statistical metrics to identify changes is affected
866 by the spread, overlap and shape of the peaks. Thus, there is an intrinsic bias in any age
867 distribution under investigation. Future research on this issue could bring significant
868 contribution to minimize this bias in a quantitative way. It also reinforces the non-uniqueness
869 of solutions to (un)mixing age distributions as highlighted by several authors (e.g., Sundell and
870 Saylor, 2017).

871 It is important to consider the implications of some of our assumptions, in particular
872 regarding the transfer of zircon from gravel to sand. In our model, we assume that all products
873 of abrasion are in the sand fraction, and that the zircons are homogeneously distributed in this
874 sand. In reality, the fraction finer than 2 mm is far more heterogeneous than assumed here, both
875 in the initial sediment supply from the hillslope to the river and in the fluvial sediment
876 transported (Attal and Lavé, 2006, Attal et al., 2015; Riebe et al., 2015, Lukens et al., 2016,
877 Sklar et al., 2017). In addition, abrasion will also produce fragments and particles in a wide
878 range of sizes, leading to potentially different mineral compositions depending on the fraction
879 sampled. For example, the abrasion of granite tends to produce sand, whereas abrasion of
880 limestone will produce more silt and clay (Bradley, 1970; Attal and Lavé, 2009). However,
881 given that no constraints about the grain size of abrasion products in the Marsyandi watershed
882 exist, we cannot estimate quantitatively how distorted our own analyses can be due to this
883 process. We must also mention that an important covariation exists between grain size of
884 abrasion products, abrasion rates and hillslope grain size supply (Attal and Lavé, 2006). Less
885 resistant bedrock types are more likely to have higher weathering rates and to produce regolith
886 with higher content of fine material (i.e., sand, silt and clay) than hard rock types, leading to

lower initial gravel supply to the river channels and consequently smaller amount of gravel available for abrasion. The covariation of hillslope grain size, grain size of abrasion products and abrasion rate associated with a given rock type can produce unusual effects, as shown in Section 4.2, and requires further attention. Because most detrital studies focus on a given sediment fraction (usually sand), it is becoming increasingly important to understand the production and evolution of the fine fraction of the sediment spectrum, from the hillslopes to the sedimentary basin, as a result of chemical and physical processes (Sklar et al., 2017); including abrasion during fluvial transport.

Hydrodynamic fractionation of grain sizes, whereby larger sediment grains travel slower than smaller ones, operates on a range of scales (bedload versus suspended load, as well as differences within bedload and within suspended load) in the majority of natural environments (e.g., Miller et al., 2014). Recent findings suggest potential bias from downstream hydraulic sorting in cases where a relationship between zircon grain age and size exists, e.g., larger grains are younger and smaller ones are older (Yang et al., 2012). The influence of grain density is also important, given that relative enrichment in gravel bars, river pools and other common sampling sites for detrital studies can bias denser minerals such as zircon. However, because our work focuses only on one type of mineral (zircon) and uses the relative proportions of zircons from different units, it seems reasonable to assume that zircons from all units will be affected in a similar way and that the outcomes of our work would not be significantly affected by the processes mentioned above, except in a case where zircons from different units have different sizes, which we cannot assess.

Finally, although we applied the same procedure adopted by Amidon et al. (2005a) to directly compare our results with theirs and assess the influence of abrasion, our no-abrasion model produces mixing proportions and relative erosion rates that are slightly different from their no-abrasion model results. Our predictions are different by 2 % and 4 % in the mixing proportions and erosion rates estimated for site E. At the sampling site G, our predictions differ by up to 2 % and 5 % in the mixing proportion and erosion rates, respectively. At the outlet (K), these differences become higher, reaching up to 6 % in the mixing proportion and 5 % in the relative erosion rates. A possible explanation for these differences is small changes in the quality of the Digital Elevation Model and/or in the minimization procedures adopted. In all cases, however, our no-abrasion model mirrors the same pattern of zircon mixing proportion and erosion estimated by the no-abrasion model of Amidon et al. (2005a).

5 Conclusion

Our numerical simulations provide evidence of the role of pebble abrasion in distorting detrital grain age information from modern sands. This distortion is significant in settings with large contrasts in rock strength or short catchments. In long catchments with no resistant lithologies, most of the gravel initially supplied from the hillslopes will have been turned into sand by the time it reaches the outlet, leading to the release of most detrital grains and limited bias potential from abrasion. Conversely, gravel from resistant lithologies (e.g., quartzite, volcanics, mica-poor granite or gneiss) can persist for transport distances of hundreds of km, locking detrital minerals within them and increasing the bias potential from abrasion: abrasion will likely lead to the underrepresentation of units characterised by such resistant rock in a sand sample. We find however that pebble abrasion is the factor with the lowest distortion capability when compared with other well-known factors that might bias the preserved sedimentary record (i.e., relative erosion rates, zircon fertility and hillslope gravel supply). Abrasion has a non-linear impact on the mixing proportion of river sand, and this impact is modulated by the initial gravel supply: whereas a doubling a zircon fertility or erosion rate in a unit will lead to a doubling of the zircon contribution from this unit in a mixed sample, the impact of doubling the abrasion rate may be much lower. We find, in one of our scenarios, that the equivalent effect of having rocks from one unit abraded 200 times faster than rocks from other units can be replicated by tripling the fertility or erosion rate of this unit.

The relative erosion rates of source units estimated by inverse modelling are impacted by abrasion, despite minimal (statistically insignificant) variations in the grain age distributions. In the Marsyandi catchment, our abrasion model predicts erosion rates that are closer to those found by the majority of previous studies, compared to a no-abrasion model. These results suggest that even when statistics are not able to identify significant changes in the age distribution of samples, the erosion rates deconvolved from them can still be significantly affected. Therefore, assessing the influence of abrasion on the evolution of the composition of river sediment is essential if we are to accurately estimate erosion rates from inverse modelling, using detrital methods based on a given sediment fraction (e.g., sand), in particular when the source units feature large variations in rock strength.

We identify research into the trade-offs between initial gravel supply and abrasion rates and into the size distribution of the products of abrasion for rocks of different lithologies as priorities to develop models that would better constrain the influence of abrasion and other factors on biases in detrital studies.

Acknowledgments

The topographic data used in this paper is freely available from <http://www.opentopography.org>. All the code used to perform our analysis as well as to generate the figures is open source and can be downloaded from GitHub at <https://github.com/clavarini>. This research is supported by the CAPES Brazilian foundation through Ph.D. scholarships provided to two of the authors (grants BEX 13193-13-9 to C.L. and 0061-13-1 to C.A.d.C.F.). The authors would like to thank David Whipp and two anonymous reviewers for their useful comments. We thank the Associate Editor Jon Warrick and the Editor Giovanni Coco for their additional comments. We are extremely grateful to William Amidon for providing the U-Pb Marsyandi's river dataset.

References

- Aguilar, G., S. Carretier, V. Regard, R. Vassallo, R. Riquelme, and J. Martinod (2014), Grain size-dependent ^{10}Be concentrations in alluvial stream sediment of the Huasco valley, a semi-arid andes region, *Quaternary Geochronology*, *19*, 163–172, doi: [10.1016/j.quageo.2013.01.011](https://doi.org/10.1016/j.quageo.2013.01.011)
- Alizai, A., A. Carter, P. D. Clift, S. VanLaningham, J. C. Williams, and R. Kumar (2011), Sediment provenance, reworking and transport processes in the Indus River by U–Pb dating of detrital zircon grains, *Global and Planetary Change*, *76*(1), 33–55.
- Allen, P. A., J. J. Armitage, A. C. Whittaker, N. A. Michael, D. Roda-Boluda, and M. D'Arcy (2015), Fragmentation model of the grain size mix of sediment supplied to basins, *The Journal of Geology*, *123*(5), 405–427.
- Amelin, Y., D.-C. Lee, A. N. Halliday, and R. T. Pidgeon (1999), Nature of the Earth's earliest crust from hafnium isotopes in single detrital zircons, *Nature*, *399*(6733), 252–255.
- Amidon, W. H., D. W. Burbank, and G. E. Gehrels (2005a), Construction of detrital mineral populations: insights from mixing of U–Pb zircon ages in Himalayan rivers, *Basin Research*, *17*(4), 463–485.
- Amidon, W. H., D. W. Burbank, and G. E. Gehrels (2005b), U–Pb zircon ages as a sediment mixing tracer in the Nepal Himalaya, *Earth and Planetary Science Letters*, *235*(1), 244–260.
- Attal, M., and J. Lavé (2006), Changes of bedload characteristics along the Marsyandi River (central Nepal): Implications for understanding hillslope sediment supply, sediment load evolution along fluvial networks, and denudation in active orogenic belts, *Geological Society of America Special Papers*, *398*, 143–171.

- Attal, M., J. Lavé, and J.-P. Masson (2006), New facility to study river abrasion processes, *Journal of Hydraulic Engineering*, 132(6), 624–628.
- Attal, M., and J. Lavé (2009), Pebble abrasion during fluvial transport: Experimental results and implications for the evolution of the sediment load along rivers, *Journal of Geophysical Research: Earth Surface*, 114(F4).
- Attal, M., S. M. Mudd, M. D. Hurst, B. Weinman, K. Yoo, and M. Naylor (2015), Impact of change in erosion rate and landscape steepness on hillslope and fluvial sediments grain size in the Feather River basin (Sierra Nevada, California), *Earth Surface Dynamics*, 3(1), 201–222, doi: 10.5194/esurf-3-201-2015
- Blum, M., and M. Pecha (2014), Mid-Cretaceous to Paleocene North American drainage reorganization from detrital zircons, *Geology*, 42(7), 607–610.
- Bradley, W. C. (1970), Effect of weathering on abrasion of granitic gravel, Colorado River (Texas), *Geological Society of America Bulletin*, 81, 61–80, doi:10.1130/0016-7606(1970)81(61:EOWOAO)2.0.CO;2
- Burbank, D., A. Blythe, J. Putkonen, B. Pratt-Sitaula, et al. (2003), Decoupling of erosion and precipitation in the Himalaya, *Nature*, 426(6967), 652.
- Campbell, I. H., P. W. Reiners, C. M. Allen, S. Nicolescu, and R. Upadhyay (2005), He–Pb double dating of detrital zircons from the Ganges and Indus rivers: implication for quantifying sediment recycling and provenance studies, *Earth and Planetary Science Letters*, 237(3), 402–432, doi: 10.1016/j.epsl.2005.06.043
- Carretier, S., V. Regard, R. Vassallo, G. Aguilar, J. Martinod, R. Riquelme, F. Christophoul, R. Charrier, E. Gayer, M. Farías, L. Audin, and C. Lagane (2015), Differences in ¹⁰Be concentrations between river sand, gravel and pebbles along the western side of the central Andes, *Quaternary Geochronology*, 27, 33–51, doi: 10.1016/j.quageo.2014.12.002
- Casagli, N., L. Ermini, L., and G. Rosati (2003), Determining grain size distribution of the material composing landslide dams in the Northern Apennines: sampling and processing methods, *Engineering Geology*, 69, 83–97, doi:10.1016/S0013-7952(02)00249-1
- Codilean, A. T., C. R. Fenton, D. Fabel, P. Bishop, and S. Xu (2014), Discordance between cosmogenic nuclide concentrations in amalgamated sands and individual fluvial pebbles in an arid zone catchment, *Quaternary Geochronology*, 19, 173–180, doi: 10.1016/j.quageo.2012.04.007

- Cox, S. E., S. N. Thomson, P. W. Reiners, S. R. Hemming, and T. van de Flierdt (2010), Extremely low long-term erosion rates around the Gamburtsev mountains in interior east Antarctica, *Geophysical Research Letters*, 37(22), L22307.
- Deal, E., A.-C. Favre, and J. Braun (2017), Rainfall variability in the Himalayan orogeny and its relevance to erosion processes, *Water Resources Research*, 53(5), 4004–4021, [doi:10.1002/2016WR020030](https://doi.org/10.1002/2016WR020030)
- Dhuime, B., C. J. Hawkesworth, P. A. Cawood, and C. D. Storey (2012), A change in the geodynamics of continental growth 3 billion years ago, *Science*, 335(6074), 1334–1336.
- Dickinson, W. R. (2008), Impact of differential zircon fertility of granitoid basement rocks in North America on age populations of detrital zircons and implications for granite petrogenesis, *Earth and Planetary Science Letters*, 275(1), 80–92, [doi: 10.1016/j.epsl.2008.08.003](https://doi.org/10.1016/j.epsl.2008.08.003)
- Dingle, E. H., M. Attal, and H. D. Sinclair (2017), Abrasion-set limits on Himalayan gravel flux, *Nature*, 544(7651), 471–474, [doi: 10.1038/nature22039](https://doi.org/10.1038/nature22039)
- Domokos, G., and G. W. Gibbons (2012), The evolution of pebble size and shape in space and time, *Proceedings of the Royal Society of London A: Mathematical, Physical and Engineering Sciences*, 468(2146), 3059–3079.
- Domokos, G., D. J. Jerolmack, A. Á. Sipos, and Á. Török, (2014), How river rocks round: resolving the shape-size paradox, *PloS One*, 9(2), e8865, <https://doi.org/10.1371/journal.pone.0088657>
- Fedo, C. M., K. N. Sircombe, and R. H. Rainbird (2003), Detrital zircon analysis of the sedimentary record, *Reviews in Mineralogy and Geochemistry*, 53(1), 277–303.
- Gabet, E. J., D. W. Burbank, B. Pratt-Sitaula, J. Putkonen, and B. Bookhagen (2008), Modern erosion rates in the high Himalayas of Nepal, *Earth and Planetary Science Letters*, 267(3), 482 – 494.
- Garzanti, E., G. Vezzoli, S. Andò, J. Lavé, M. Attal, C. France-Lanord, and P. DeCelles (2007), Quantifying sand provenance and erosion (Marsyandi River, Nepal Himalaya), *Earth and Planetary Science Letters*, 258(3), 500–515.
- Garzanti, E., S. Andò, and G. Vezzoli (2008), Settling equivalence of detrital minerals and grain size dependence of sediment composition, *Earth and Planetary Science Letters*, 273(1), 138–151.

- Garzanti, E., S. Andò, and G. Vezzoli (2009), Grain size dependence of sediment composition and environmental bias in provenance studies, *Earth and Planetary Science Letters*, 277(3), 422–432.
- Gehrels, G., P. Kapp, P. DeCelles, A. Pullen, R. Blakey, A. Weislogel, L. Ding, J. Guynn, A. Martin, N. McQuarrie, et al. (2011), Detrital zircon geochronology of pre-Tertiary strata in the Tibetan-Himalayan orogen, *Tectonics*, 30(5).
- Gehrels, G. E. (2000), Introduction to detrital zircon studies of Paleozoic and Triassic strata in western Nevada and northern California, *Special Paper of the Geological Society of America*, 347, 1–17.
- Glotzbach, C., F. Busschers, and J. Winsemann (2017), Detrital thermochronology of Rhine, Elbe and Meuse river sediment (central Europe): Implications for provenance, erosion and mineral fertility, *International Journal of Earth Sciences*, doi: [10.1007/s00531-017-1502-9](https://doi.org/10.1007/s00531-017-1502-9)
- Haddadchi, A., D. S. Ryder, O. Evrard, and J. Olley (2013), Sediment fingerprinting in fluvial systems: review of tracers, sediment sources and mixing models, *International Journal of Sediment Research*, 28(4), 560 – 578.
- Haddadchi, A., J. Olley, and P. Laceby (2014), Accuracy of mixing models in predicting sediment source contributions, *Science of The Total Environment*, 497, 139 – 152.
- Hodges, K., C. Wobus, K. Ruhl, T. Schildgen, and K. Whipple (2004), Quaternary deformation, river steepening, and heavy precipitation at the front of the higher Himalayan ranges, *Earth and Planetary Sciences Letters*, 220(3-4), 379–389, doi: 10.1016/S0012-821X(04)00063-9
- Iizuka, T., T. Komiya, S. Rino, S. Maruyama, and T. Hirata (2010), Detrital zircon evidence for Hf isotopic evolution of granitoid crust and continental growth, *Geochimica et Cosmochimica Acta*, 74(8), 2450 – 2472.
- Kimbrough, D. L., M. Grove, G. E. Gehrels, R. J. Dorsey, K. A. Howard, O. Lovera, A. Aslan, P. K. House, and P. A. Pearthree (2015), Detrital zircon U-Pb provenance of the Colorado River: A 5 m.y. record of incision into cover strata overlying the Colorado plateau and adjacent regions, *Geosphere*, 11(6), 1719, doi: 10.1130/GES00982.1
- Kirstein, L.A., M.G. Fellin, S.D. Willett, A. Carter, Y.G. Chen, J.I. Garver, D-C. Lee (2009), Pliocene onset of rapid exhumation in Taiwan during arc-continent collision: New insights from detrital thermochronometry, *Basin Research*, 22(3), 270 – 285 DOI: 10.1111/j.1365-2117.2009.00426.x

- Kirstein, L.A., A. Carter, Y.G. Chen (2013), Impacts of arc collision on small orogens: New insights from the Coastal Range detrital record, Taiwan, *Journal of the Geological Society, London*, 171(1), 5-8, DOI: 10.1144/jgs2013-046
- Krumbein, W. C. (1941), The effects of abrasion on the size, shape and roundness of rock fragments, *The Journal of Geology*, 49(5), 482–520.
- Kuenen, P. H. (1956), Experimental abrasion of pebbles: 2. rolling by current, *The Journal of Geology*, 64(4), 336–368.
- Lawrence, R. L., R. Cox, R. W. Mapes, and D. S. Coleman (2011a), Hydrodynamic fractionation of zircon age populations, *Geological Society of America Bulletin*, 123(1-2), 295–305.
- Lawrence, R. L., R. Cox, R. W. Mapes, and D. S. Coleman (2011b), Hydrodynamic fractionation of zircon age populations, *GSA Bulletin*, 123(1-2), 295, [doi: 10.1130/B30151.1](https://doi.org/10.1130/B30151.1)
- Le Bouteiller, C., F. Naaim-Bouvet, N. Mathys, and J. Lavé (2011), A new framework for modeling sediment fining during transport with fragmentation and abrasion, *Journal of Geophysical Research: Earth Surface*, 116(F3), F03002.
- Le Fort, P. (1975), Himalaya: the collided range. Present knowledge of the continental arc, *American Journal of Science*, 275(1), 1–44.
- Lewin, J., and P. A. Brewer (2002), Laboratory simulation of clast abrasion, *Earth Surface Processes and Landforms*, 27(2), 145–164.
- Licht, A., A. Pullen, P. Kapp, J. Abell, and N. Giesler (2016), Eolian cannibalism: Reworked loess and fluvial sediment as the main sources of the Chinese Loess plateau, *Geological Society of America Bulletin*, 128(5-6), 944, [doi: 10.1130/B31375.1](https://doi.org/10.1130/B31375.1)
- Lukens, C. E., C. S. Riebe, L. S. Sklar, and D. L. Shuster (2016), Grain size bias in cosmogenic nuclide studies of stream sediment in steep terrain, *Journal of Geophysical Research: Earth Surface*, 121(5), 978–999, [doi: 10.1002/2016JF003859](https://doi.org/10.1002/2016JF003859)
- Malusà, M. G., A. Carter, M. Limoncelli, I. M. Villa, and E. Garzanti (2013), Bias in detrital zircon geochronology and thermochronometry, *Chemical Geology*, 359, 90–107.
- Malusà, M. G., A. Resentini, and E. Garzanti (2016), Hydraulic sorting and mineral fertility bias in detrital geochronology, *Gondwana Research*, 31, 1–19.
- Miller, K. L., T. Szabó, D. J. Jerolmack, and G. Domokos (2014), Quantifying the significance of abrasion and selective transport for downstream fluvial grain size evolution, *Journal of Geophysical Research: Earth Surface*, 119(11), 2412–2429.

1112 Mills, H. H. (1979), Downstream rounding of pebbles—A quantitative review, *Journal of*
1113 *Sedimentary Research*, 49(1).

1114 Moecher, D. P., and S. D. Samson (2006), Differential zircon fertility of source terranes and
1115 natural bias in the detrital zircon record: Implications for sedimentary provenance analysis,
1116 *Earth and Planetary Science Letters*, 247(3), 252–266.

1117 Mojzsis, S. J., T. M. Harrison, and R. T. Pidgeon (2001), Oxygen-isotope evidence from ancient
1118 zircons for liquid water at the Earth's surface 4,300 Myr ago, *Nature*, 409(6817), 178–181.

1119 Nocedal, J., and S. Wright (2000), *Numerical Optimization (Springer Series in Operations*
1120 *Research and Financial Engineering)*, Springer.

1121 Olen, S. M., B. Bookhagen, B. Hoffmann, D. Sachse, D. P. Adhikari, and M. R. Strecker (2015),
1122 Understanding erosion rates in the Himalayan orogen: A case study from the Arun valley,
1123 *Journal of Geophysical Research: Earth Surface*, 120(10), 2080–2102, doi:
1124 [10.1002/2014JF003410](https://doi.org/10.1002/2014JF003410)

1125 Oliver, G., K. Zaw, M. Hotson, S. Meffre, and T. Manka (2014), U–Pb zircon geochronology
1126 of Early Permian to Late Triassic rocks from Singapore and Johor: A plate tectonic
1127 reinterpretation, *Gondwana Research*, 26(1), 132–143.

1128 Parker, G. (1991), Selective sorting and abrasion of river gravel. I: Theory, *Journal of*
1129 *Hydraulic Engineering*, 117(2), 131–147.

1130 Perez, N. D., and B. K. Horton (2014), Oligocene-miocene deformational and depositional
1131 history of the andean hinterland basin in the northern Altiplano plateau, southern Peru,
1132 *Tectonics*, 33(9), 1819–1847, doi: [10.1002/2014TC003647](https://doi.org/10.1002/2014TC003647)

1133 Pratt-Sitaula, B., D. W. Burbank, A. Heimsath, and T. Ojha (2004), Landscape disequilibrium
1134 on 1000–10,000 year scales Marsyandi river, Nepal, central Himalaya, *Geomorphology*,
1135 58(1), 223 – 241.

1136 Riebe, C. S., L. S. Sklar, C. E. Lukens, and D. L. Shuster (2015), Climate and topography
1137 control the size and flux of sediment produced on steep mountain slopes, *Proceedings of the*
1138 *National Academy of Sciences*, 112(51), 15,574–15,579, doi: [10.1073/pnas.1503567112](https://doi.org/10.1073/pnas.1503567112)

1139 Satkoski, A. M., Wilkinson, B. H., Hietpas, J., & Samson, S. D. (2013). Likeness among detrital
1140 zircon populations—An approach to the comparison of age frequency data in time and space.
1141 *Bulletin*, 125(11-12), 1783-1799. <https://doi.org/10.1130/B30888.1>

1142 Saylor, J. E., and K. E. Sundell (2016), Quantifying comparison of large detrital geochronology
1143 data sets, *Geosphere*, 12(1), 203–220, doi: [10.1130/GES01237.1](https://doi.org/10.1130/GES01237.1)

- Saylor, J. E., D. F. Stockli, B. K. Horton, J. Nie, and A. Mora (2012), Discriminating rapid exhumation from syndepositional volcanism using detrital zircon double dating: Implications for the tectonic history of the Eastern Cordillera, Colombia, *Geological Society of America Bulletin*, 124(5-6), 762–779.
- Saylor, J. E., J. N. Knowles, B. K. Horton, J. Nie, and A. Mora (2013), Mixing of source populations recorded in detrital zircon U-Pb age spectra of modern river sands, *The Journal of Geology*, 121(1), 17–33.
- Schumm, S., and M. Stevens (1973), Abrasion in place: a mechanism for rounding and size reduction of coarse sediments in rivers, *Geology*, 1(1), 37–40.
- Sharman, G. R., and S. A. Johnstone (2017), Sediment unmixing using detrital geochronology, *Earth and Planetary Science Letters*, 477, 183–194, [doi: 10.1016/j.epsl.2017.07.044](https://doi.org/10.1016/j.epsl.2017.07.044)
- Singh, S. K., S. K. Rai, and S. Krishnaswami (2008), Sr and Nd isotopes in river sediments from the Ganga basin: Sediment provenance and spatial variability in physical erosion, *Journal of Geophysical Research: Earth Surface*, 113(F3), F03006.
- Sklar, L. S., and W. E. Dietrich (2001), Sediment and rock strength controls on river incision into bedrock, *Geology*, 29(12), 1087–1090.
- Sklar, L. S., and W. E. Dietrich (2004), A mechanistic model for river incision into bedrock by saltating bed load, *Water Resources Research*, 40(6).
- Sklar, L. S., C. S. Riebe, J. A. Marshall, J. Genetti, S. Leclere, C. L. Lukens, and V. Mercres (2017), The problem of predicting the size distribution of sediment supplied by hillslopes to rivers, *Geomorphology*, 277, 31–49, [doi: 10.1016/j.geomorph.2016.05.005](https://doi.org/10.1016/j.geomorph.2016.05.005)
- Stephens, M. A. (1970), Use of the Kolmogorov-Smirnov, Cramér-Von Mises and related statistics without extensive tables, *Journal of the Royal Statistical Society. Series B (Methodological)*, pp. 115–122.
- Sundell, K. E., and J. E. Saylor (2017), Unmixing detrital geochronology age distributions, *Geochemistry, Geophysics, Geosystems*, [doi: 10.1002/2016GC006774](https://doi.org/10.1002/2016GC006774).
- Thomson, S. N., P. W. Reiners, S. R. Hemming, and G. E. Gehrels (2013), The contribution of glacial erosion to shaping the hidden landscape of East Antarctica, *Nature Geoscience*, 6(3), 203.
- Tochilin, C. J., P. W. Reiners, S. N. Thomson, G. E. Gehrels, S. R. Hemming, and E. L. Pierce (2012), Erosional history of the Prydz Bay sector of East Antarctica from detrital apatite and zircon geo- and thermochronology multidating, *Geochemistry, Geophysics, Geosystems*, 13(11), Q11015.

1177 Vermeesch, P. (2012), On the visualisation of detrital age distributions, *Chemical Geology*, 312,
1178 190–194, [doi: 10.1016/j.chemgeo.2012.04.021](https://doi.org/10.1016/j.chemgeo.2012.04.021).
1179 Vermeesch, P. (2013). Multi-sample comparison of detrital age distributions. *Chemical*
1180 *Geology*, 341, 140–146. <https://doi.org/10.1016/j.chemgeo.2013.01.010>
1181 Wilde, S. A., J. W. Valley, W. H. Peck, and C. M. Graham (2001), Evidence from detrital
1182 zircons for the existence of continental crust and oceans on the Earth 4.4 Gyr ago, *Nature*,
1183 409(6817), 175–178.
1184
1185
1186

TABLES

Table 1: Published parameters used in this work to predict the mixing proportion and relative distribution of erosion rates at sampling points in the Marsyandi watershed.

Source ^a	Zircon fertility (grains/g) ^b	Abrasion rate (% mass loss/km) ^c	Gravel supply (%) ^d
TTS	0.6	4.3	75
MG	0	0.4	75
F II-III	0.3	0.4	75
F I	0.8	1.4	75
LH	0.3	9.4	75

^a TTS = Tethyan series, MG = Manaslu granite, F II-III = Formation II-III, F I = Formation I, LH = Lesser Himalaya.

^b Estimated by Amidon et al. [2005a].

^c Estimated from experimental abrasion rates by Attal and Lavé [2006].

^d Average percentage of hillslope supply coarser than sand (i.e., > 2 mm), estimated by Attal and Lavé [2006].

Table 2: Parameters used in the numerical experiments testing the influence of pebble abrasion rates in the age distribution of sands. TTS = Tethyan Series, F II-III = Formation II-III, F I = Formation I, LH = Lesser Himalaya.

Experiment	Zircon fertility (grains/g) ^a	Abrasion rate (% mass loss/km) ^b			
		TTS	F II-III	F I	LH
A1	1	0.4	0.4	0.4	0.4
A2	1	31	0.15	0.15	0.15
A3	1	0.15	0.15	0.15	31
A4	1	4.3	0.4	1.4	9.4

^a Estimated by Amidon et al. [2005a].

^b Estimated by Attal and Lavé [2006].

Table 3: Parameters used in the numerical experiments comparing the distortion caused by well-known controlling factors (erosion rate, zircon fertility, hillslope gravel supply and abrasion). TTS = Tethyan Series, F II-III = Formation II-III, F I = Formation I, LH = Lesser Himalaya. A sensitivity analysis was also carried out for experiments B2 to B5b, with results shown in Figure 4: TTS' abrasion rate was varied between 0.15 and 31 %/km in B2; TTS' erosion rate was varied between 1 and 5.1 mm/yr in B3; fertility of non-TTS units was varied between 0 and 0.8 grains/g in B4; gravel supply from TTS and LH was varied between 60 and 90 % in B5 and B5b, respectively.

Experiment	Factor	Coefficients			
		TTS	F II-III	F I	LH
B1	All uniform - no abrasion				
B2	Abrasion rate (% mass loss/km)	31	0.15	0.15	0.15
B3	Erosion rate (mm/a)	5.1	1	1	1
B4	Zircon fertility (grains/g)	0.8	0	0	0
B5	Gravel supply (%)	60	90	90	90
B5b*	Gravel supply (%)	90	90	90	60
B6	Gravel supply (%) + Abrasion rate (% mass loss/km)	60 31	90 0.15	90 0.15	90 0.15

* B5b is similar to B5 except that LH has the smallest gravel supply instead of TTS; see text for details.

FIGURE CAPTION

Figure 1. Conceptual representation of the variables used in the abrasion mixing model and the resulting impact on the modelled U-Pb detrital age distribution $z(x)$ used to estimate erosion rates. In this representation, different travelled distances d impact the proportion of sand sourced from the two units. This leads to a change in the zircon mixing proportion Φ_i^Z that modifies the detrital age distribution $z(x)$ in the 63-125 μm fraction used in geochronology. (a) Controlling factors of mass and zircon concentration of sands in the abrasion model: top – bedrock control: exposure area (km^2) and mineral fertility (grains/g); bottom – sediment control: hillslope gravel fraction (coarser than sand) and abrasion rate (% mass loss/km), with abrasion progressively transferring zircons from the gravel to the sand fraction as sediment is transported downstream. (b) On a spatial scale, two contributing single source units (S1 and S2) are mixed downstream (S3). Sample S3 reflects the mixture of upstream controlling factors, including abrasion; in this case, source one is over-represented as the longer transport distance leads to a greater sand production from abrasion and therefore contribution in the mixed sand sample (S3). This is exemplified by the inset (bottom left) showing the mass of sand along a linear river system coming from sources 1 and 2 in a simple model based on *Attal and Lavé's* (2006, 2009): 1000 tons of sediment are supplied to the system every km (all gravel in this scenario), from source 1 over the first 10 km and from source 2 over the next 10 km. Gravel is abraded according to the Sternberg's law (see text) at a rate of 2 % mass loss/km. Total amount of sand (black) is sum of sand from sources 1 (pink) and 2 (purple). The contribution from source 1 in a sand sample is shown by green dashed line; it is 72% after a distance of 20 km (sample S3). As gravel from source 1 experienced greater transport distance, more sand has been released from source 1 compared to source 2.

Figure 2. Source units of the Marsyandi watershed and their U-Pb detrital age distribution. (a) Geological map for the Marsyandi watershed superimposed on hillshade derived from 30-m resolution Shuttle Radar Topography Mission (SRTM) data. Geological units are derived from *Le Fort* (1975) (see also *Amidon et al.*, 2005a, and *Attal and Lavé*, 2006). Sample locations and U-Pb detrital ages distributions (samples A to K) measured by *Amidon et al.* (2005a) are also indicated; they are used in this work as a study case and in the numerical simulations. Grey PDFs indicate mixed samples, whereas coloured PDFs represent source samples, with the colour relating to the unit in question. MCT is Main Central Thrust; STD 1 and 2 are South

Tibetan Detachment as mapped by *Searle and Godin* (2003), and *Colchen et al.* (1987), respectively. (b) Synthetic U-Pb age distributions (samples 1-5) created in this work to facilitate the statistical assessment of our numerical experiments: samples 1 to 4 are sources (indicated by colours) and sample 5 is mixed sand sample predicted at outlet without abrasion (location K in (a)). The vertical axis in the PDFs is relative probability ($\times 10^{-3}$) and the horizontal axis is U-Pb grain age (Ga).

Figure 3. Results of the numerical simulations that tested the statistics of synthetic U-Pb zircon age populations (PDPs) derived from zircon mixing modelling using abrasion scenarios (Table 2): uniform abrasion rate (A1), very high abrasion rate for TTS (A2) or for LH (A3), and realistic values for the different units based on *Attal and Lavé* (2006) (A4). (a) Percentage zircon from the different rock units in sand at the catchment outlet. Mixing proportions in the no-abrasion case reflect the relative exposure area of the different units; dashed lines indicate change with respect to the no-abrasion scenario. (b) and (d) Probability density plots (PDPs) generated using the mixing proportions predicted by the abrasion model on synthetic and natural age distribution, respectively. Arrows identify peaks associated with the four sources. (c) and (e) Statistical assessment of the PDPs through PDF cross-plots. Additional statistical assessment (e.g., Q-Q plots) can be found in the supporting information (Table S5, S6, Fig. S2). Note that scenarios A2 and A3 lead to the greatest amount of distortion with the synthetic dataset (see R^2 values in (c)), with greater distortion in case A2 due to the TTS peak being isolated compared to the LH peak. With the natural dataset, only scenario A3 leads to a significant amount of distortion compared to the other scenarios (see R^2 values in (e)), which we explain by LH having a unique peak at ~ 1.8 Ga; most TTS peaks are shared with other units.

Figure 4. Synthetic zircon age populations (PDPs) derived from zircon mixing in numerical experiments B2-B6 (Table 3), showing sensitivity of PDPs to (a) abrasion (B2), (b) erosion rate (B3), (c) fertility (B4) and (d-e) hillslope gravel supply (B5-B5b). An additional experiment B6 has a low initial gravel supply and high abrasion rate for TTS (Table 3). B1 is the reference case (all factors uniform, no abrasion); B2 is the same as simulation A2. Note the quasi linear response to erosion rate, fertility and hillslope gravel supply (b-e), in stark contrast with the influence of abrasion rate (a). Combining low gravel supply with high abrasion rate leads to increased distortion (f): TTS is overrepresented in a sand sample at the outlet with respect to other units, due to both greater sand contribution at the source (hillslope) and greater release of

sand through abrasion of gravel (high abrasion rate). Full statistical assessment can be found in the supporting information (Table S7-S8).

Figure 5. (a, c) Probability density plots (PDPs) and (b, d) PDF cross-plots of the end-member scenarios from experiments B2-B6 (Table 3). (a, b) are based on synthetic age distributions. (c, d) are based on natural age distributions. Additional statistical assessment can be found in the supporting information (Table S7-S8, Fig. S4). Note the clear distortion generated by the different parameters with the synthetic dataset (b); the distortion is not as significant with the natural dataset (d), which we explain as due to overlapping peaks, though the relative influence of the different parameters is the same in both datasets (with fertility having the greatest effect).

Figure 6. Results of the numerical simulations comparing the capability of each controlling factor to reproduce the distortions of abrasion (B2), erosion (B3), fertility (B4) and hillslope gravel supply (B5b) in the zircon age populations (PDPs). (a, c) Probability density plots (PDPs) of the experiments, comparing the distribution created by varying a given factor (grey) with the best fit distributions obtained by varying one of the other parameters (curves). Factors that can perfectly reproduce the distribution are grouped in “Others”. (b, d) PDF cross-plots and their R^2 comparing how the (tested) factors can reproduce a distortion caused by a specific (targeted) factor; thickness of circles refers to scenario, whereas colour refers to tested factor. (a, b) are based on synthetic age distributions. (c, d) are based on natural age distributions. Note the similar performance (R^2) with both synthetic and natural datasets. Additional statistical assessment can be found in the supporting information (Table S9, S10).

Figure 7. Results of the numerical mixing models for the Marsyandi uppermost sampling site (E): resulting U-Pb age distributions (PDPs), relative erosion rates and statistical assessment. (a) Percentage zircon from the different rock units in sand at site E (pink) and predicted relative erosion rates (blue) for the no-abrasion and abrasion models; dashed lines indicate change with respect to the best-fit approach (see text). (b) PDPs of the measured grains, modelled best-fit, no-abrasion and abrasion models. (c) PDF cross-plots comparing the modelled PDFs (no abrasion and abrasion) to the best-fit PDF (in blue and green) as well as comparing the modelled PDFs among themselves (in yellow); key shows “X-axis PDF” x “Y-axis PDF”.

Figure 8. Results of the numerical mixing models for the intermediate Marsyandi sampling site (G): their resulting age distributions (PDPs), relative erosion and statistical assessment. (a) Percentage zircon from the different rock units in sand at site G (pink) and predicted relative erosion rates (blue) for the no-abrasion and abrasion models; dashed lines indicate change with respect to the best-fit approach (see text). (b) PDPs of the measured grains, modelled best-fit, no-abrasion and abrasion models. (c) PDF cross-plots comparing the modelled PDFs (no-abrasion and abrasion) to the best-fit PDF (in blue and green) as well as comparing the modelled PDFs among themselves (in yellow); key shows “X-axis PDF” x “Y-axis PDF”.

Figure 9. Results of the numerical mixing models for the Marsyandi outlet (K): their resulting age distributions (PDPs), relative erosion and statistical assessment. A) Percentage zircon from the different rock units in sand at site K (pink) and predicted relative erosion rates (blue) for the no-abrasion and abrasion models; dashed lines indicate change with respect to the best-fit approach (see text). B) PDPs of the measured grains, modelled best-fit, no-abrasion and abrasion models. C) PDF cross-plots comparing the modelled PDFs (no-abrasion and abrasion) to the best-fit PDF (in blue and green) as well as comparing the modelled PDFs among themselves (in yellow) ; key shows “X-axis PDF” x “Y-axis PDF”.

Figure 10. (a) Schematic diagram summarising the circumstances under which bias from abrasion can be expected in a sand sample. Bias is expected to decrease with increasing length of the river system, as the relative amount of sand (and therefore zircons or any other tracer minerals) retained in gravel decreases downstream. How quickly sand is released from gravel through abrasion is a function of the abrasion rate, so “short” and “long” have relative meanings for a catchment (*, see (b)). Strong contrast in rock resistance to abrasion will enhance bias, as gravel from hard lithologies will persist for long distances, therefore limiting the release of zircon or any other tracer minerals from this lithology (in the figure, rock type 2 is harder, leading to underrepresentation in sand sample). (b) Downstream conversion from gravel to sand as a function of abrasion rate (note log scale on x-axis). These results are based on a simple linear river model from *Attal and Lavé’s* (2006, 2009) (see also Fig. 1b): a given amount of sediment is supplied to the system every km and gravel is abraded according to Sternberg’s law. At a distance of 10 km downstream, 61 % of all gravel supplied to the system has been turned into sand for a mass loss of 20 %/km (39 % of gravel remaining). This figure is 10 %

and 1 % for a mass loss of 2 and 0.2 %/km, respectively. At a distance of 100 km, nearly all gravel supplied to the system has been turned into sand for a mass loss of 20 %/km (4 % of gravel remaining). This figure is 58 % and 9 % for a mass loss of 2 and 0.2 %/km, respectively. Gravel from resistant lithologies can persist over hundreds of km. (c) Influence of abrasion rate and initial gravel fraction on relative contribution of abrasion to sand. Key is as in (b): abrasion rate of 0.2, 2 and 20 %/km are shown by solid (light blue), short dash (dark brown) and long dash (black) lines, respectively. % value on curves indicates initial gravel fraction from hillslopes. Curves show the relative contribution of sand from abrasion in a sand sample taken at a given distance downstream.

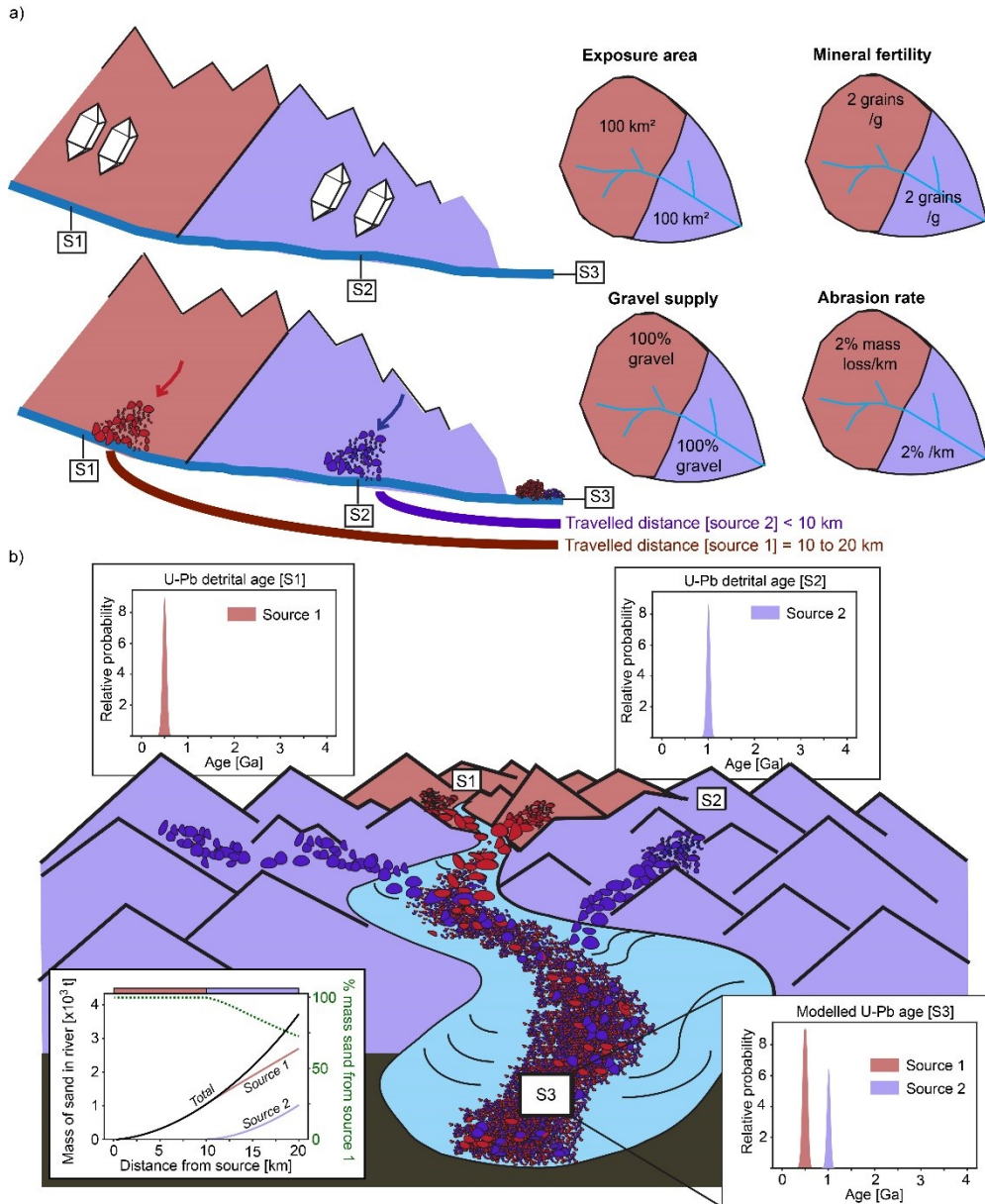


Figure 1. Conceptual representation of the variables used in the abrasion mixing model and the resulting impact on the modelled U-Pb detrital age distribution $z(x)$ used to estimate erosion rates. In this representation, different travelled distances d impact the proportion of sand sourced from the two units. This leads to a change in the zircon mixing proportion Φ_i^Z that modifies the detrital age distribution $z(x)$ in the 63-125 μm fraction used in geochronology. (a) Controlling factors of mass and zircon concentration of sands in the abrasion model: top – bedrock control: exposure area (km^2) and mineral fertility (grains/g); bottom – sediment control: hillslope gravel fraction (coarser than sand) and abrasion rate (% mass loss/km), with abrasion progressively transferring zircons from the gravel to the sand fraction as sediment is transported downstream. (b) On a spatial scale, two contributing single source units (S1 and S2) are mixed downstream (S3). Sample S3 reflects the mixture of upstream controlling factors, including abrasion; in this case, source one is over-represented as the longer transport distance leads to a greater sand production from abrasion and therefore contribution in the mixed sand sample (S3). This is exemplified by the inset (bottom left) showing the mass of sand along a linear river system coming from sources 1 and 2 in a simple model based on *Attal and Lavé's* (2006, 2009): 1000 tons of sediment are supplied to the system every km (all gravel in this scenario), from source 1 over the first 10 km and from source 2 over the next 10 km. Gravel is abraded according to the Sternberg's law (see text) at a rate of 2 % mass loss/km. Total amount of sand (black) is sum of sand from sources 1 (pink) and 2 (purple). The contribution from source 1 in a sand sample is shown by green dashed line; it is 72% after a distance of 20 km (sample S3). As gravel from source 1 experienced greater transport distance, more sand has been released from source 1 compared to source 2.

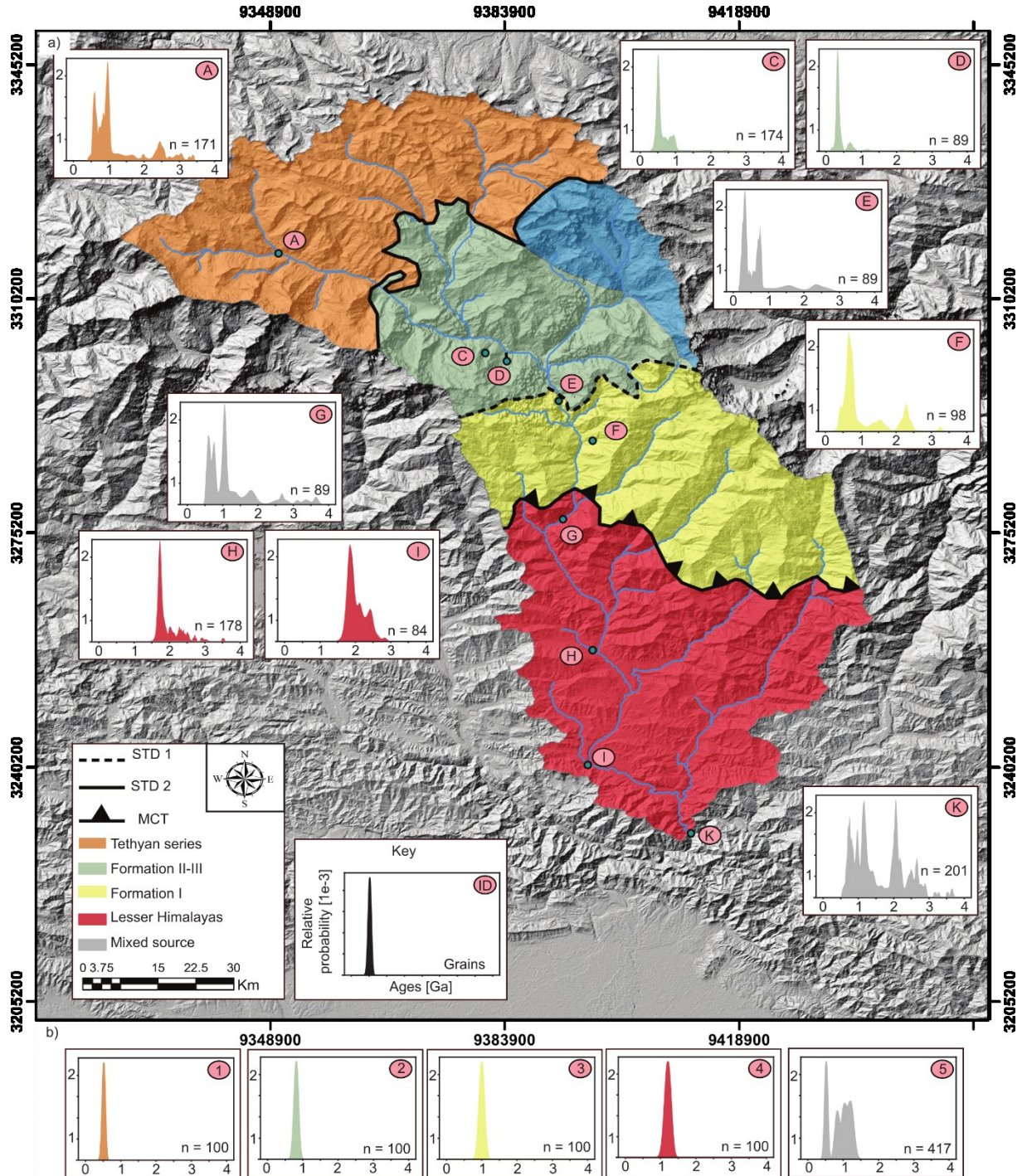


Figure 2. Source units of the Marsyandi watershed and their U-Pb detrital age distribution. (a) Geological map for the Marsyandi watershed superimposed on hillshade derived from 30-m resolution Shuttle Radar Topography Mission (SRTM) data. Geological units are derived from *Le Fort* (1975) (see also *Amidon et al.*, 2005a, and *Attal and Lavé*, 2006). Sample locations and U-Pb detrital ages distributions (samples A to K) measured by *Amidon et al.* (2005a) are also indicated; they are used in this work as a study case and in the numerical simulations. Grey PDFs indicate mixed samples, whereas coloured PDFs represent source samples, with the colour relating to the unit in question. MCT is Main Central Thrust; STD 1 and 2 are South Tibetan Detachment as mapped by *Searle and Godin* (2003), and *Colchen et al.* (1987), respectively. (b) Synthetic U-Pb age distributions (samples 1-5) created in this work to facilitate the statistical assessment of our numerical experiments: samples 1 to 4 are sources (indicated by colours) and sample 5 is mixed sand sample predicted at outlet without abrasion (location K in (a)). The vertical axis in the PDFs is relative probability ($\times 10^{-3}$) and the horizontal axis is U-Pb grain age (Ga).

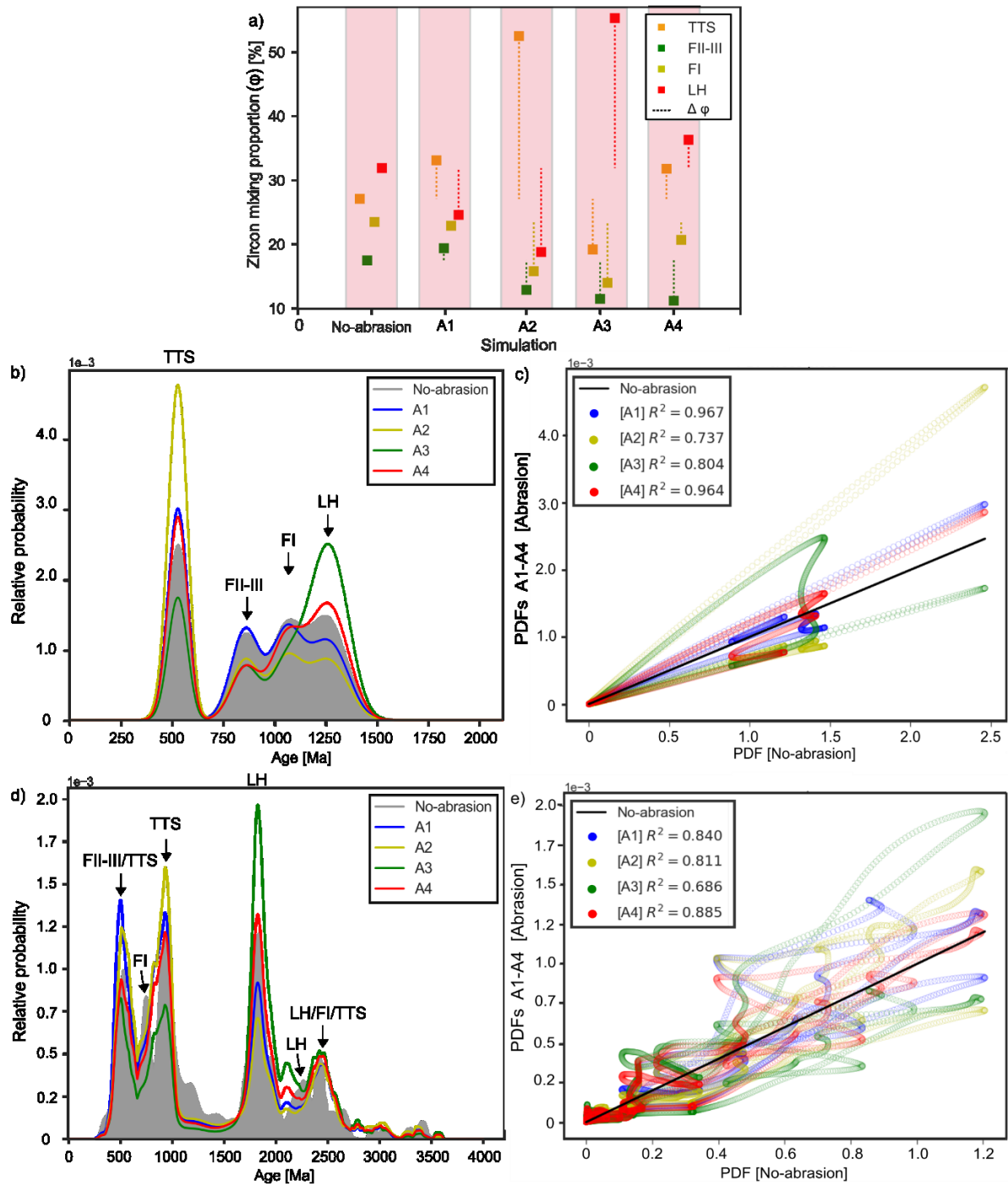


Figure 3. Results of the numerical simulations that tested the statistics of synthetic U-Pb zircon age populations (PDPs) derived from zircon mixing modelling using abrasion scenarios (Table 2): uniform abrasion rate (A1), very high abrasion rate for TTS (A2) or for LH (A3), and realistic values for the different units based on *Attal and Lavé* (2006) (A4). (a) Percentage zircon from the different rock units in sand at the catchment outlet. Mixing proportions in the no-abrasion case reflect the relative exposure area of the different units; dashed lines indicate change with respect to the no-abrasion scenario. (b) and (d) Probability density plots (PDPs) generated using the mixing proportions predicted by the abrasion model on synthetic and natural age distribution, respectively. Arrows identify peaks associated with the four sources. (c) and (e) Statistical assessment of the PDPs through PDF cross-plots. Additional statistical assessment (e.g., Q-Q plots) can be found in the supporting information (Table S5, S6, Fig. S2). Note that scenarios A2 and A3 lead to the greatest amount of distortion with the synthetic dataset (see R^2 values in (c)), with greater distortion in case A2 due to the TTS peak being isolated compared to the LH peak. With the natural dataset, only scenario A3 leads to a significant amount of distortion compared to the other scenarios (see R^2 values in (e)), which we explain by LH having a unique peak at ~ 1.8 Ga; most TTS peaks are shared with other units.

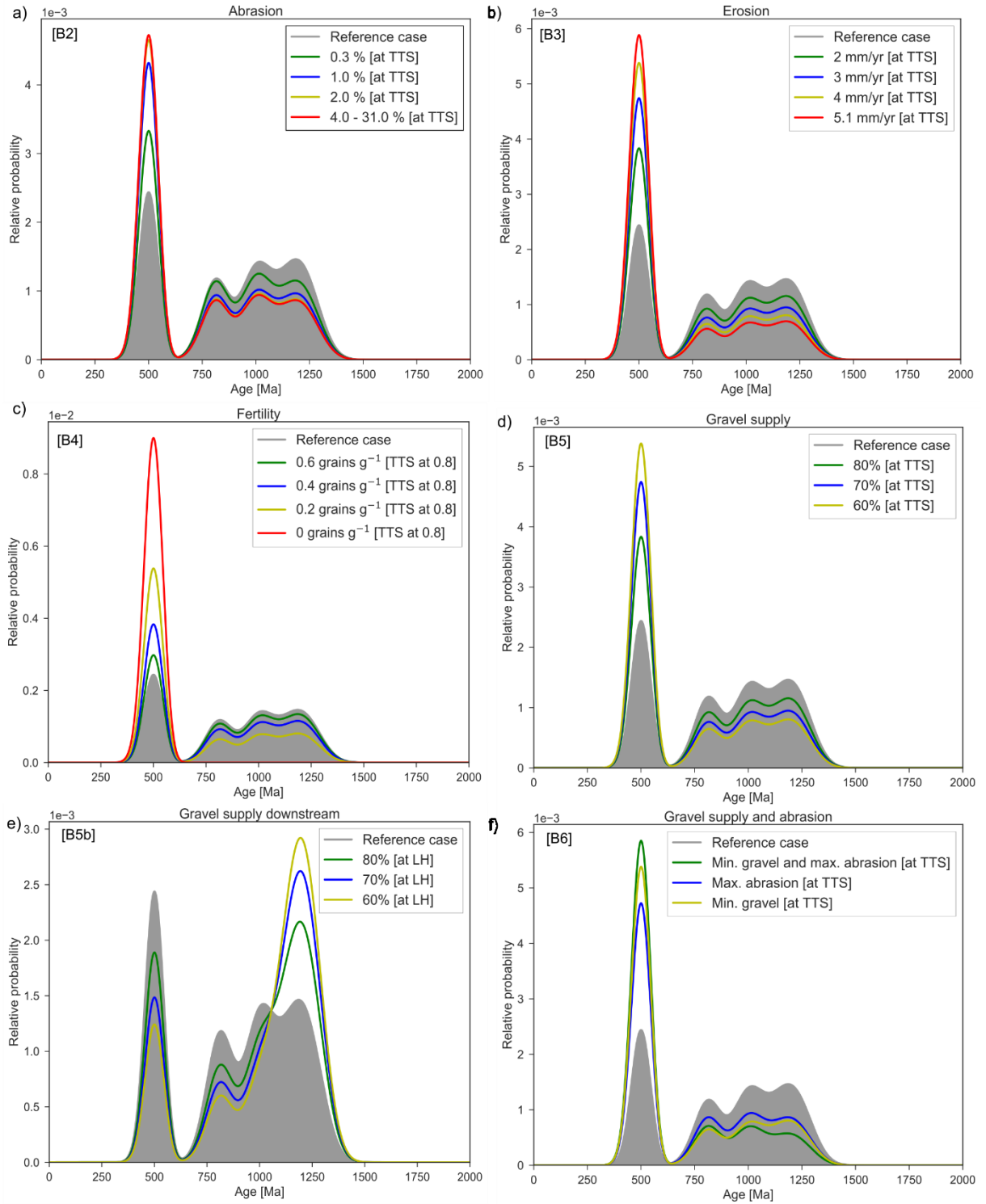


Figure 4. Synthetic zircon age populations (PDPs) derived from zircon mixing in numerical experiments B2-B6 (Table 3), showing sensitivity of PDPs to (a) abrasion (B2), (b) erosion rate (B3), (c) fertility (B4) and (d-e) hillslope gravel supply (B5-B5b). An additional experiment B6 has a low initial gravel supply and high abrasion rate for TTS (Table 3). B1 is the reference case (all factors uniform, no abrasion); B2 is the same as simulation A2. Note the quasi linear response to erosion rate, fertility and hillslope gravel supply (b-e), in stark contrast with the influence of abrasion rate (a). Combining low gravel supply with high abrasion rate leads to increased distortion (f): TTS is overrepresented in a sand sample at the outlet with respect to other units, due to both greater sand contribution at the source (hillslope) and greater release of sand through abrasion of gravel (high abrasion rate). Full statistical assessment can be found in the supporting information (Table S7-S8).

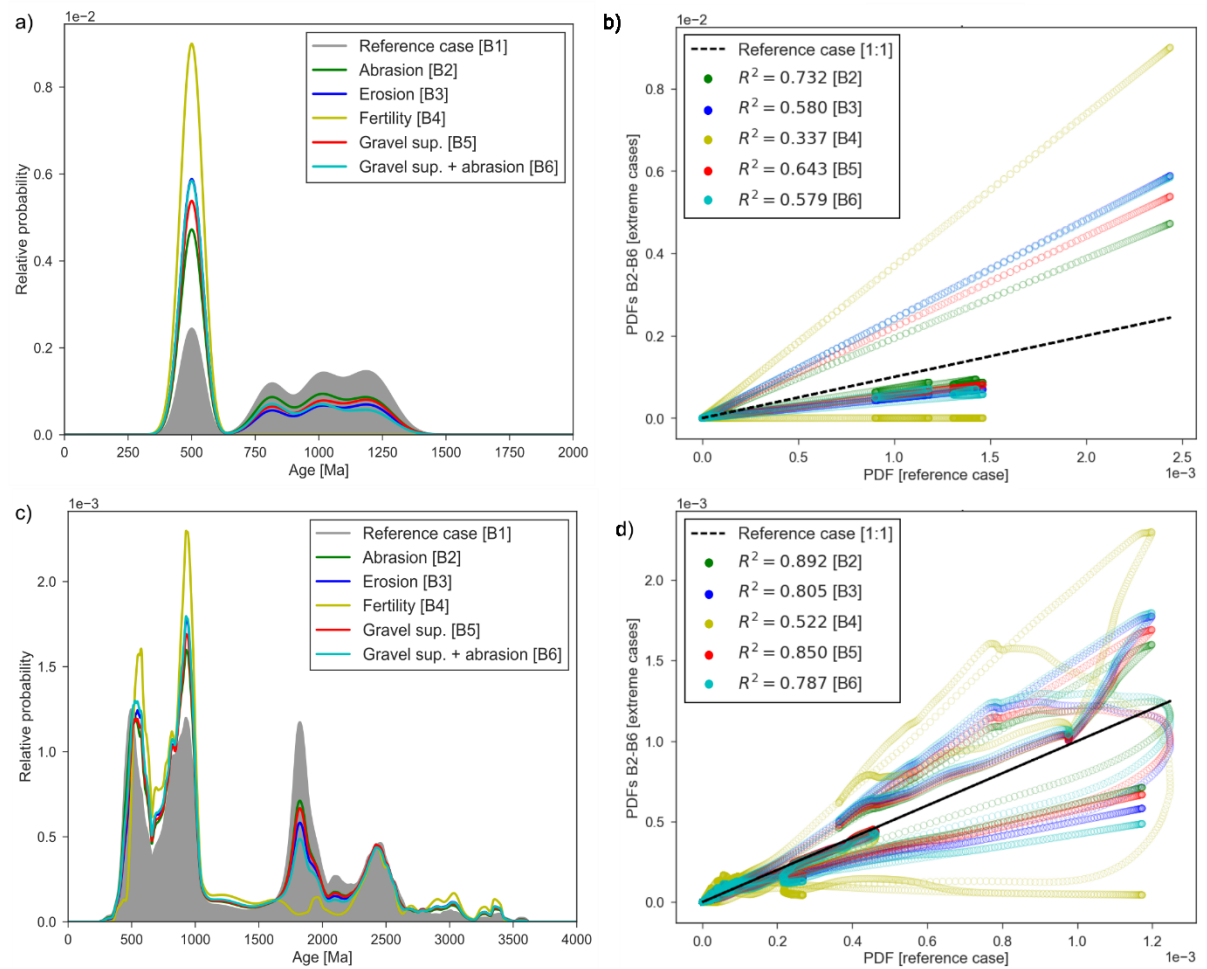


Figure 5. (a, c) Probability density plots (PDPs) and (b, d) PDF cross-plots of the end-member scenarios from experiments B2-B6 (Table 3). (a, b) are based on synthetic age distributions. (c, d) are based on natural age distributions. Additional statistical assessment can be found in the supporting information (Table S7-S8, Fig. S4). Note the clear distortion generated by the different parameters with the synthetic dataset (b); the distortion is not as significant with the natural dataset (d), which we explain as due to overlapping peaks, though the relative influence of the different parameters is the same in both datasets (with fertility having the greatest effect).

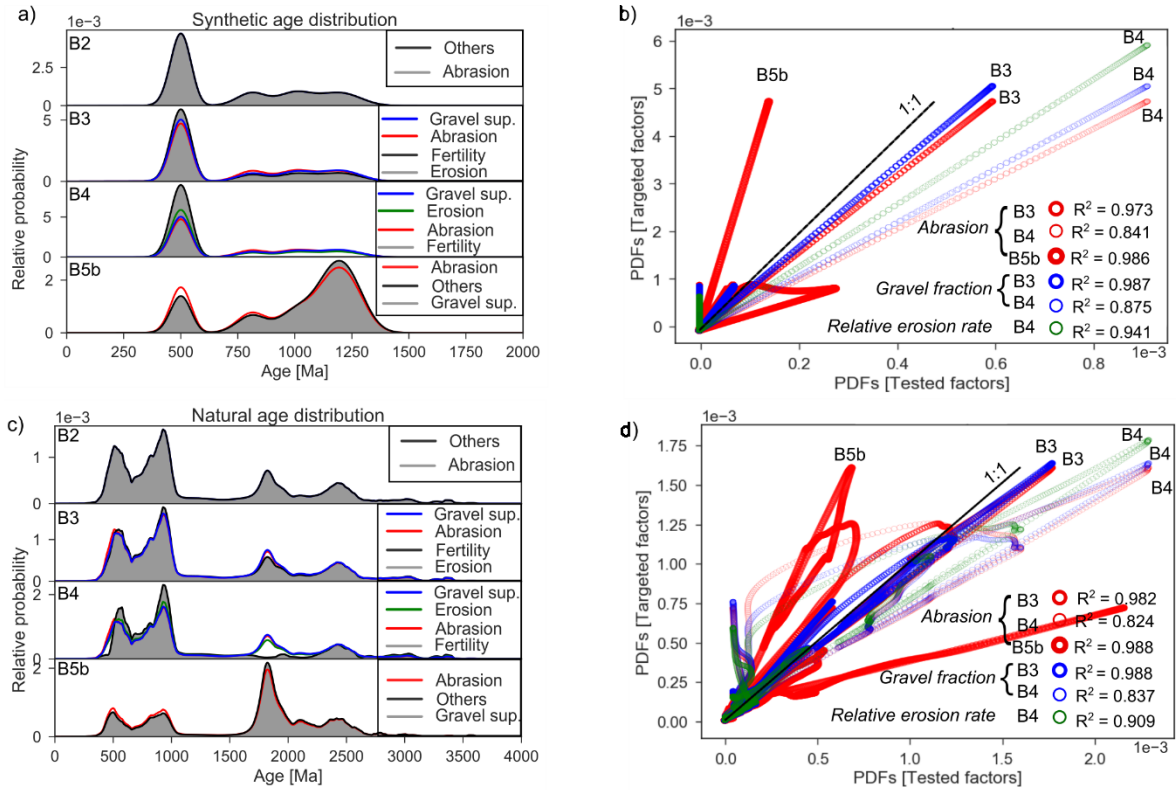


Figure 6. Results of the numerical simulations comparing the capability of each controlling factor to reproduce the distortions of abrasion (B2), erosion (B3), fertility (B4) and hillslope gravel supply (B5b) in the zircon age populations (PDPs). (a, c) Probability density plots (PDPs) of the experiments, comparing the distribution created by varying a given factor (grey) with the best fit distributions obtained by varying one of the other parameters (curves). Factors that can perfectly reproduce the distribution are grouped in “Others”. (b, d) PDF cross-plots and their R^2 comparing how the (tested) factors can reproduce a distortion caused by a specific (targeted) factor; thickness of circles refers to scenario, whereas colour refers to tested factor. (a, b) are based on synthetic age distributions. (c, d) are based on natural age distributions. Note the similar performance (R^2) with both synthetic and natural datasets. Additional statistical assessment can be found in the supporting information (Table S9, S10).

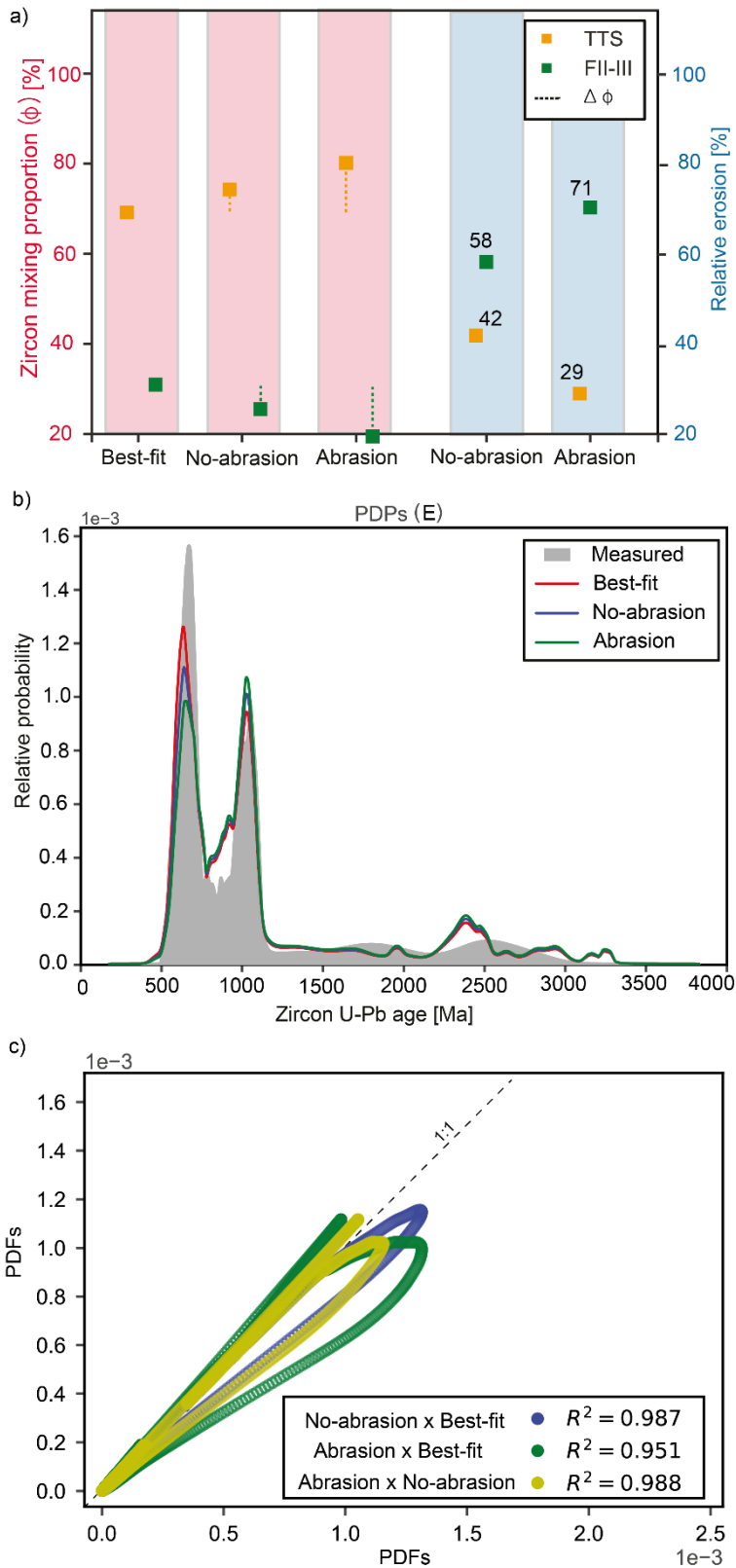


Figure 7. Results of the numerical mixing models for the Marsyandi uppermost sampling site (E): resulting U-Pb age distributions (PDPs), relative erosion rates and statistical assessment. (a) Percentage zircon from the different rock units in sand at site E (pink) and predicted relative erosion rates (blue) for the no-abrasion and abrasion models; dashed lines indicate change with respect to the best-fit approach (see text). (b) PDPs of the measured grains, modelled best-fit, no-abrasion and abrasion models. (c) PDF cross-plots comparing the modelled PDFs (no abrasion and abrasion) to the best-fit PDF (in blue and green) as well as comparing the modelled PDFs among themselves (in yellow); key shows “X-axis PDF” x “Y-axis PDF”.

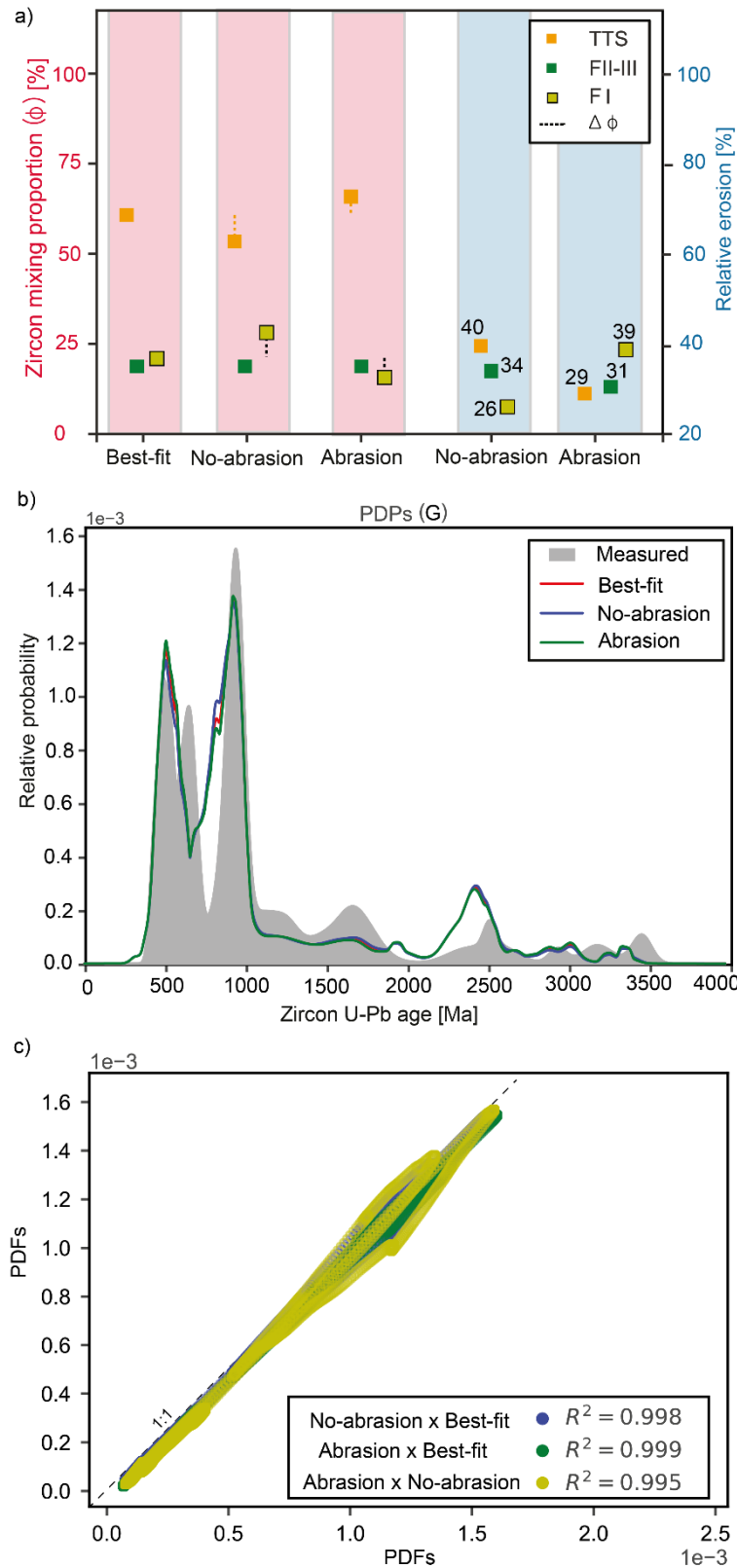


Figure 8. Results of the numerical mixing models for the intermediate Marsyandi sampling site (G): their resulting age distributions (PDPs), relative erosion and statistical assessment. (a) Percentage zircon from the different rock units in sand at site G (pink) and predicted relative erosion rates (blue) for the no-abrasion and abrasion models; dashed lines indicate change with respect to the best-fit approach (see text). (b) PDPs of the measured grains, modelled best-fit, no-abrasion and abrasion models. (c) PDF cross-plots comparing the modelled PDFs (no-abrasion and abrasion) to the best-fit PDF (in blue and green) as well as comparing the modelled PDFs among themselves (in yellow); key shows “X-axis PDF” x “Y-axis PDF”.

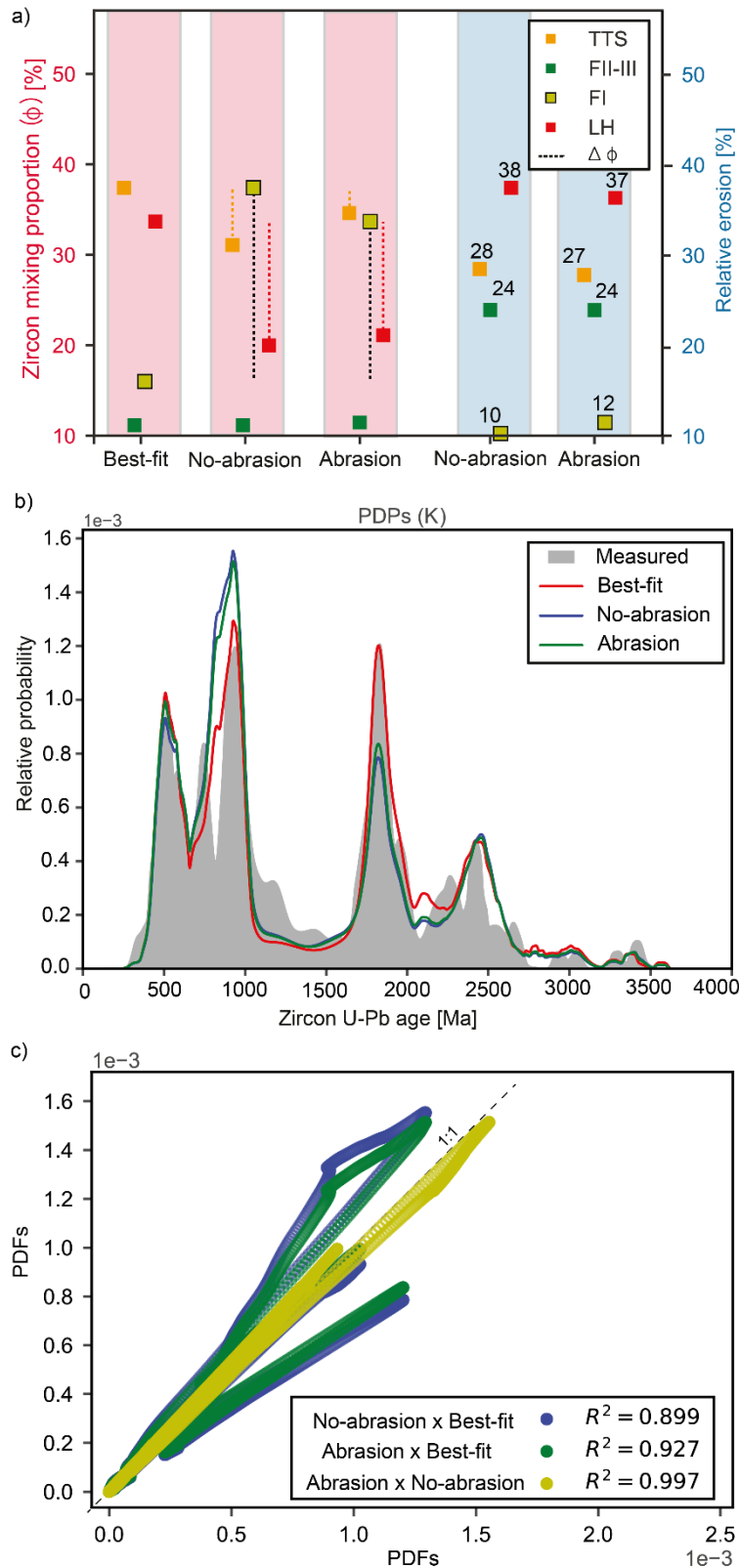


Figure 9. Results of the numerical mixing models for the Marsyandi outlet (K): their resulting age distributions (PDPs), relative erosion and statistical assessment. A) Percentage zircon from the different rock units in sand at site K (pink) and predicted relative erosion rates (blue) for the no-abrasion and abrasion models; dashed lines indicate change with respect to the best-fit approach (see text). B) PDPs of the measured grains, modelled best-fit, no-abrasion and abrasion models. C) PDF cross-plots comparing the modelled PDFs (no-abrasion and abrasion) to the best-fit PDF (in blue and green) as well as comparing the modelled PDFs among themselves (in yellow) ; key shows “X-axis PDF” x “Y-axis PDF”.

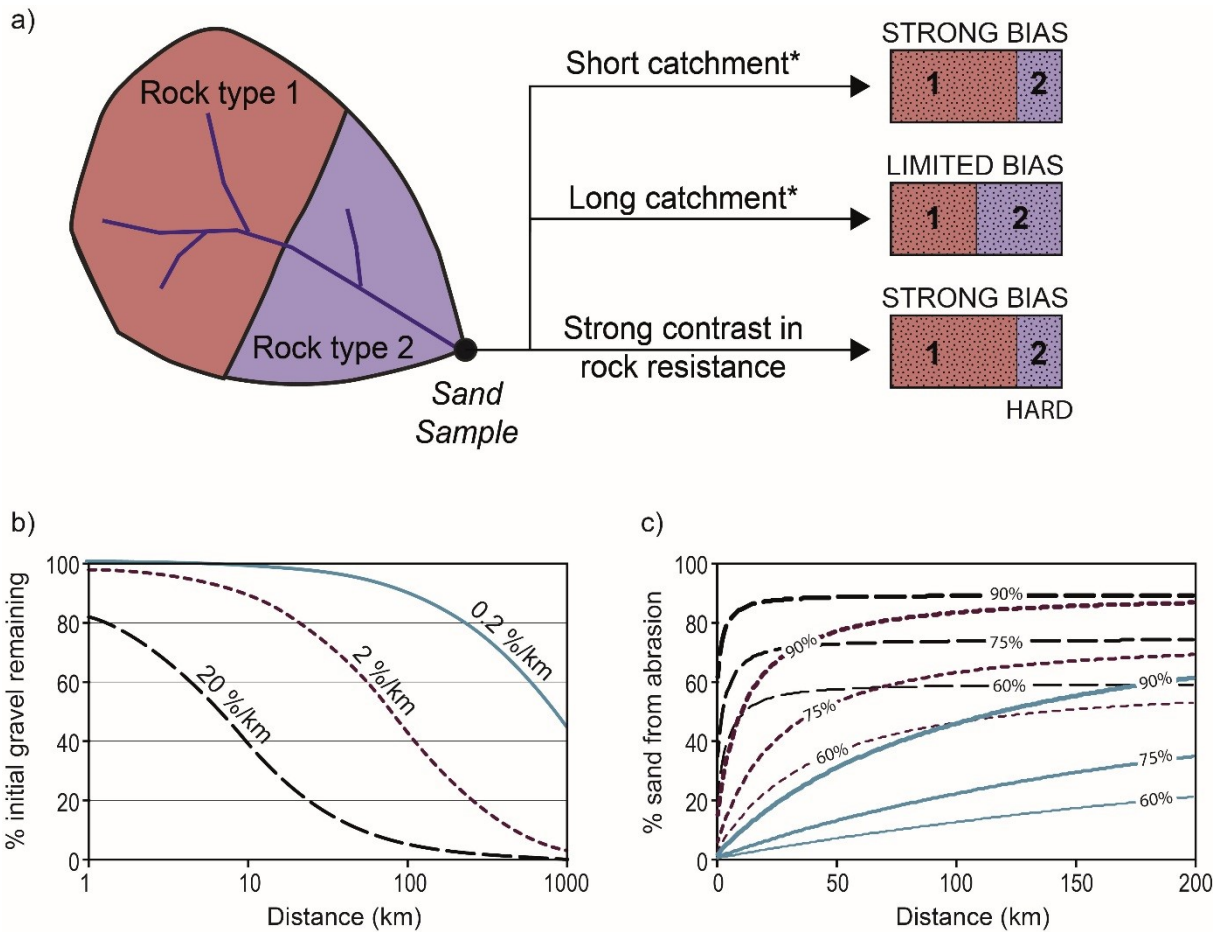


Figure 10. (a) Schematic diagram summarising the circumstances under which bias from abrasion can be expected in a sand sample. Bias is expected to decrease with increasing length of the river system, as the relative amount of sand (and therefore zircons or any other tracer minerals) retained in gravel decreases downstream. How quickly sand is released from gravel through abrasion is a function of the abrasion rate, so “short” and “long” have relative meanings for a catchment (*, see (b)). Strong contrast in rock resistance to abrasion will enhance bias, as gravel from hard lithologies will persist for long distances, therefore limiting the release of zircon or any other tracer minerals from this lithology (in the figure, rock type 2 is harder, leading to underrepresentation in sand sample). (b) Downstream conversion from gravel to sand as a function of abrasion rate (note log scale on x-axis). These results are based on a simple linear river model from *Attal and Lavé’s* (2006, 2009) (see also Fig. 1b): a given amount of sediment is supplied to the system every km and gravel is abraded according to Sternberg’s law. At a distance of 10 km downstream, 61 % of all gravel supplied to the system has been turned into sand for a mass loss of 20 %/km (39 % of gravel remaining). This figure is 10 % and 1 % for a mass loss of 2 and 0.2 %/km, respectively. At a distance of 100 km, nearly all gravel supplied to the system has been turned into sand for a mass loss of 20 %/km (4 % of gravel remaining). This figure is 58 % and 9 % for a mass loss of 2 and 0.2 %/km, respectively. Gravel from resistant lithologies can persist over hundreds of km. (c) Influence of abrasion rate and initial gravel fraction on relative contribution of abrasion to sand. Key is as in (b): abrasion rate of 0.2, 2 and 20 %/km are shown by solid (light blue), short dash (dark brown) and long dash (black) lines, respectively. % value on curves indicates initial gravel fraction from hillslopes. Curves show the relative contribution of sand from abrasion in a sand sample taken at a given distance downstream.